

Dear editor and reviewer,

We appreciate your helpful and constructive comments that improved our manuscript. We have made a point-by-point reply to the comments and revised all editorial corrections suggested from you and Dr. Booth. The original comments are shown below in black, while the responses to the comments follow in blue. A marked-up manuscript is attached at the end of this reply.

### Reviews from Adam Booth

Review of revised manuscript, “Antarctic ice sheet thickness estimation using the H/V spectral ratio method with single-station seismic ambient noise” (Yan et al.)

I thank the authors for their careful response to my first review. I’m glad to see that my comments were considered and pleased that the authors found them useful.

There is one point from my previous comment that I think the authors might have misunderstood, partly due to a poor choice of words on my part. When I commented “How big a problem would terrain corrections specifically be in Antarctica?”, referring to a L54 of the paper, I was suggesting that they would unlikely be a problem over ice sheets since they are rather flat. Therefore, even if high-resolution topography data were unavailable, the terrain correction would not be significantly impeded. However, I do agree with the authors correction anyway, that high-resolution data will benefit the terrain correction, so I’m not sure any amendment is actually needed.

All of my remaining comments are straightforward – I don’t anticipate that any of them would represent a particularly significant stumbling block.

1. Abstract: “In this study” is not required. *(Line 13)*
2. L58 “...and are relatively cost-efficient” *(Line 59)*
3. L76 “properties to a few metres depth” *(Line 77)*
4. L129-130. Change the sentence to “The peak in the H/V spectrum may also be followed by a trough.” *(Line 132)*
5. L133-136. Unclear what is meant in this sentence; check the grammar. *(Line 135-137)*
6. L152 – lower case ‘w’ in ‘where’. *(Line 156)*
7. L155. Is anisotropy really meant to be a case of a complicated “sedimentary structure”? Do you just mean the anisotropy of the ice?
8. L181-2. “such as studies of thickness and shear-wave velocities.” This can be removed; you have already established that these are the key inferences from the H/V method. *(Line 195-196)*
9. L264 – “identified the resonance frequency”, or (probably better) “identified resonance frequencies.” *(Line 279)*
10. L295 – “in consistence” should be “consistent”. *(Line 314)*
11. L299 – “thickness was used”. (Line 318)
12. L327 – should be “inverted” rather than “inversion”? *(Line 347)*
13. 344-5 – “can be effectively used”? *(Line 368)*
14. 353 – missing character; should it be “~” *(Lin3 377)*
15. L374 – is “obtaining abundant results” necessary to include? Just say that there have been many

methods applied. (*Line 397-400*)

16. Figure 2 caption. "...are referred to Wittlinger (2012)." should be "...are consistent with Wittlinger (2012)." (*Line 593*)

Response: As all Dr. Booth's comments except for the 7th one are straightforward and very reasonable, we therefore just revised each of them accordingly. These revisions are indicated by the line numbers (*the number refers to this marked-up manuscript and it is the same hereafter*). As for the 7th comment, sedimentary layers are generally assumed as vertical transverse isotropy (VTI) medium in depth imaging study, which will also affect the shear-wave velocity.

#### **Reviews from editor:**

Dear authors,

I received a second review from Dr. Booth. He is overall positive and made some editorial suggestions. I assessed the revised manuscript by myself as well. Revision is significant and this manuscript can be acceptable with additional revisions suggested below. Please provide a mark-up manuscript and point-to-point responses in which corresponding revisions are clearly indicated by line numbers or by pasting the revised text.

1. Expansion of the methods section 2.2 improved the manuscript significantly. The general description at lines 138-160 (in the marked up manuscript) is satisfactory. However, the revision at lines 177-200 should be improved, though I don't expect the full description of the method here. It is helpful if you mention how HV in Equation (2) and  $HV^{(theo)}$  in Equation (3) are connected in a clearer way, first of all. Sigma and m are not defined in the text. Are P1, P2, and P3 the average energy densities of a diffuse field? If so, define P more explicitly. Do you need to connect P and Green's tensor components using this equation? If so, explanation on its physical meaning is helpful.

Response: As extensive studies indicated, the Green's function links the H/V spectrum and the medium properties as the imaginary part of the Green's function is proportional to the average spectral power (or average energy density) of the ambient-vibration ground-motion. In a horizontally layered structure, the contribution of both the surface wave and the body wave to the Green's function can be computed with provided medium properties including primary- and shear-wave velocities. Thus, the theoretical H/V spectrum can be calculated with known medium properties. We have revised this part to make it clear. Specific revisions can be seen in *Line 171-185 and 191-194*.

2. Define three different H/V estimates of ice thickness more clearly, namely Equation (1), DFA + Model A, and DFA + Model B (or even define symbols). To a certain point in this manuscript, I thought that Model A is used with Equation (1), not with DFA. These estimates are stated many times but in slightly different ways and thus confusing. It's better to clearly define them once and stick with these terms.

Response: Thanks for your suggestion. The ice thickness estimations obtained from the approximation Eq. (1) and H/V spectrum inversions using model A and model B are defined as Equation (1), DFA + Model A, and DFA + Model B estimates, respectively. The citations of them have been revised thoroughly in the main texts, as well as in Table 1 and Fig. 7.

3. I am not convinced yet how independent ice-thickness estimates can be retrieved using the H/V method, because BEDMAP2 ice thicknesses are used to constrain the method (lines 229-230). What happens, if there is not such constraint? To rigorously argue this independence, it is necessary to make the H/V estimate without BEDMAP2's guidance and compare these results with BEDMAP2's ice thickness.

Response: Thanks for your constructive comment. We would like to state that the layer thickness and the shear-wave are not decoupled for the H/V method as they jointly influence the H/V spectrum. Given that the shear-wave structure of the ice sheet is clear (the average  $V_s$  is  $\sim 2.0$  km s<sup>-1</sup>), the H/V method can be used to investigate ice thickness.

Similar with the RES method that exploits two-way echo time and the electromagnetic velocity in ice, the H/V estimation using the approximation Eq. (1) is also independent. If a well-established relationship between ice sheet thickness and the shear-wave velocity has been built like that in sedimentary layer depth imaging studies, the equation alone can be used to estimate ice thickness.

As for the H/V spectrum inversion, the involvement of BEDMAP2 ice thickness can reduce the independence of its estimations. Due to the non-uniqueness of geophysical inversion, it is very helpful and sometimes necessary in some cases to exploit prior constraints to reduce the non-uniqueness. We therefore used BEDMAP2 ice thickness as references to build model spaces to conduct the H/V spectrum inversion. To respond to your comment, we think the approximate estimates obtained from Eq. (1) (that are independent from BEDMAP2 ice thickness) can also be used to serve as reference thicknesses to constrain model spaces and obtain similar results.

Rough estimation: I am not a native English speaker but I think that “approximate estimate” or “first-order estimate” can show the nature of this estimate much clearer than “rough estimate”. Maybe this is a personal taste so I leave it with the authors.

Response: Yes, we agree with your comment that “approximate estimate” is much proper. We have revised it in the texts thoroughly.

Wittlinger (2012) and Wittlinger (2015): are they Wittlinger and Farra?

Response: Yes, both Wittlinger and Farra are authors of the two literatures. We have corrected the citations in the main texts.

L141: Define SH.

Response: SH, together with SV wave, are two polarizations of shear-wave (S wave) when an incident S wave enters in a anisotropy medium. We have added some texts in the manuscript to make it clear (*Line 127*)

Lines 143-144: Revise the sentence.

Response: We have revised it to make it understandable. (*Line 130*)

Lines 188-189: check sets of parentheses and brackets to show the imaginary components.

Response: We have corrected sets of parentheses and brackets. (*Line 171,174*)

L261ff: what does this error stand for? It is said at L285-286 “Error of Thickness I is associated with BEDMAP2’s uncertainty”. Is the error of the resonance frequency here also related to BEDMAP2’s error or relevant to the quality of the resonance peak?

Response: The error stated here at L261 refers to the peak frequency standard deviation that calculated using the GEOPSY software. The mentioned “relative error of Thickness I to BEDMAP2 ice thickness”

at L285-286 (listed in column 5 in Table 1) were calculated with the equation:  $\frac{|ThicknessI - Bed2|}{Bed2} \cdot 100\%$ .

Error of Thickness I ( $\Delta h$ , listed in column 4 in Table 1) are obtained using Eq. (1) by averaging the calculated ice thickness using the peak frequency  $f_0$  and its corresponding standard deviation  $\sigma$  (i.e.

$\Delta h = \left( \left( \frac{V_S}{f_0} - \frac{V_S}{f_0 + \sigma} \right) + \left( \frac{V_S}{f_0 - \sigma} - \frac{V_S}{f_0} \right) \right) / 2$ ). We have clarified them in the Table 1 caption. **(Line 574-**

**578)**

Line 262: Fig. 3, not Fig. 2.

Response: Revised accordingly **(Line 256)**

Line 351: cite Table 1.

Response: Table 1 has been cited here. **(Line 348)**

Line 373: remove “(Fig. 5)”?

Response: Removed accordingly. **(Line 372)**

Lines 400-404: Do you really need this paragraph? I feel that this conclusion section can be stronger if you start with the second paragraph.

Response: We agree with your comment and have removed this paragraph as this paragraph is somewhat repetitive to the introduction part. **(Line 394-400)**

Table 1 caption: Please clarify thickness I and II in a better way. See the main point #2 above. Also, explain the error shown for Thickness I in the caption briefly.

Response: We have change thickness I and II to Equation (1) and DFA + Model B according to your good suggestion. The error shown in column 4 and the relative errors listed in column 5 and 7 are clarified in the caption. **(Line 575-578)**

Figure 3: change the order of individual panels or add lines between panels to group these 9 panels into 3 sub-groups. Explain what the vertical bars mean (thick gray and thin red).

Response: We have grouped the nine stations into three sub-groups that each of them belongs to one of the three seismic arrays. The vertical bar (i.e. the two vertical gray areas) stands for the peak frequency deviation domains that calculated using all the spectra with the GEOPSY software. The left gray area seems larger than the right one as they are shown on a logarithmic frequency scale. Their values are exactly the same. We have explained it in the caption. **(Line 598-602)**

Figure 4: scale all four profiles. Now the profile A-A’ takes the full page width (2 columns) for 2000 km, whereas the profile D-D’ of 1000-km long takes only about one third of the page width. The use of the

same scale is important because the H/V method can be more useful to estimate ice thickness when the topography is less variable. Please make sure that all fonts are larger than 8 pt (feel free to use full page width and height). Separately I think that it is more appropriate to show the four stations without corresponding peaks in gray, not in red, and highlight the nine representative stations presented in Fig. 3, 5, 6 (e.g. different color or thicker curve).

Response: We have modified this figure according to your suggestion. The profiles are plotted in the horizontal scale that is proportional to the actual length of the profiles, and in the vertical that is in correspondence with their elevations. However, due to the fact that the profile CC' is only 180 km long, no details can be seen when plot using the same horizontal scale. We therefore only shorten this profile to a certain extent. The other suggestions have also been revised accordingly. (*Line 612-616*)

Figures 6 and 8: Explain red and thin dotted vertical lines. If it shows what the thick brown bars in Fig. 3 show, consider using the same legends all in Figs. 3, 6, and 8.

Response: Yes, the red and thin dotted vertical lines stand for the observed peak frequency and its corresponding standard errors calculated using the GEOPSY software, respectively. However, there are five stations (ST07 here and ST04, ST06, N060, and UPTW in supplementary Fig. S4 and S5) that are in absence of peak frequencies in the observed H/V spectrum, so we calculated the expected peak frequency using its BEDMAP2 ice thickness and Eq. (1). We also assumed a 10% standard deviation for their peak frequencies. Following your helpful suggestion, we have replaced Fig. 6 and 8 (and supplementary Fig. S4 and S5) with the revised ones using similar legends with that of Fig. 3.

Figure 7: Do you really need this figure, or can you show the same information by adding the Model A estimates to Figure 4? Figure 4 already show BEDMAP2, Equation (1), and Model B estimates. If you judge that this figure is necessary, please provide justification (would the figure be too busy to read details if all info is shown in Fig. 4?). Do you really need three panels for Fig. 7? You can show BEDMAP2 using mask, and three different estimates using markers (but then such figure is very similar to the current Fig. 4). In any case, clarify how the station number is given (is it in the same order listed in Table 1?).

Response: We have tried to show all BEDMAP2, Equation (1), Model A, and Model B ice thickness estimates in Figure 4. The figure however, as you predicted, was too busy to read details since some dots that denoting particular estimates would be masked by the other dots. Additionally, only 46 stations that obtained ice thickness estimates are showing along these four profiles. We therefore think Figure 7 is necessary to show all 60 stations on one hand and in a clearer way on the other hand. We have adjusted the order to show the three panels (now in the order of Equation (1), DFA + Model A, and DFA + Model B). Besides, the station number of this figure is in the same order of the stations listed in Table 1. We have clarified it in the caption. (*Line 640*)

Figure 9: I think that this figure can easily cause misleading, because blue dots perfectly match with the interfaces and thus Wittlinger and Farra make better estimates than this study. I recommend using BEDMAP2 thickness to mask the bed and ice.

Response: The blue dots (now purple dots) separating the interface between the ice and the bed in fact is radar ice thicknesses. Wittlinger and Farra (2012, 2015) used radar ice thickness to investigate the shear-wave velocity structure in an ice sheet. Analyzing the P-wave receiver function waveforms, they found negative amplitude in the waveforms and attributed this negative amplitude to the existence of a low

shear-wave velocity layer in an ice sheet. They then investigate the shear- wave velocity structure and determined the upper and the lower ice sheet thickness using a grid search technique. This figure is plotted to show the consistence of the interface separating the upper and the lower ice layer between our results and that of Wittlinger and Farra (2012). Besides, the overall ice thickness obtained from the H/V method is generally consistent with the radar ice thickness they adopted. Following your helpful suggestion, we have changed the color of the interface to avoid misleading and clarified it in the caption. *(Line 659-664)*

#### Clarification for a mistake in Table 1

After checking this manuscript, we apologize that we paste the wrong values of Bedmap2 ice thickness and the DFA + Model B estimate of station ST03 in Table 1. The current listed values belong to station ST07 that was not listed here. We have corrected it in Table 1 and updated all corresponding texts and figures.

1  
2 **Antarctic ice sheet thickness estimation using the H/V**  
3 **spectral ratio method with single-station seismic ambient**  
4 **noise**

5 **Peng Yan<sup>1</sup>, Zhiwei Li<sup>2</sup>, Fei Li<sup>1,3\*</sup>, Yuande Yang<sup>1</sup>, Weifeng Hao<sup>1</sup>, Feng Bao<sup>2</sup>**

6 <sup>1</sup>Chinese Antarctic Center of Surveying and Mapping, Wuhan University, Wuhan 430079, China

7 <sup>2</sup>State Key Laboratory of Geodesy and Earth's Dynamics, Institute of Geodesy and Geophysics, Chinese  
8 Academy of Sciences, Wuhan 430077, China

9 <sup>3</sup>State Key Laboratory of Information Engineering in Surveying, Mapping and Remote Sensing, Wuhan  
10 University, Wuhan 430079, China

11 *Correspondence to:* Fei Li (fli@whu.edu.cn)

12  
13 **Abstract.** ~~In this study, w~~We report on a successful application of the horizontal-to-vertical spectral ratio (H/V)  
14 method, generally used to investigate the subsurface velocity structures of the shallow crust, to estimate the  
15 Antarctic ice sheet thickness for the first time. Using three-component, five-day long, seismic ambient noise  
16 records gathered from more than 60 temporary seismic stations located on the Antarctic ice sheet, the ice  
17 thickness measured at each station has comparable accuracy to the Bedmap2 database. Preliminary analysis  
18 revealed that 60 out of 65 seismic stations on the ice sheet obtained clear peak frequencies ( $f_0$ ) related to the ice  
19 sheet thickness in the H/V spectrum. Thus, assuming that the isotropic ice layer lies atop a high velocity  
20 half-space bedrock, the ice sheet thickness can be calculated by a simple approximation formula. About half of  
21 the calculated ice sheet thickness were consistent with the Bedmap2 ice thickness values. To further improve the  
22 reliability of ice thickness measurements, two-type models were built to fit the observed H/V spectrum through  
23 non-linear inversion. The two-type models represent the isotropic structures of single- and two-layer ice sheet,  
24 and the latter depicts the non-uniform, layered characteristics of the ice sheet widely distributed in Antarctica.  
25 The inversion results suggest that the ice thicknesses derived from the two-layer ice models were in good  
26 consistence with the Bedmap2 ice thickness database, and their ice thickness differences were within 300 m at  
27 almost all stations. Our results support previous finding that the Antarctic ice sheet is stratified. Extensive data  
28 processing indicates that the time length of seismic ambient noise records can be shortened to two hours for  
29 reliable ice sheet thickness estimation using the H/V method. This study extends the application fields of the  
30 H/V method and provides an effective and independent way to measure ice sheet thickness in Antarctica.

## 1 Introduction

The Antarctic ice sheet is the largest on the Earth, covering over 98 % of Antarctic continent. As a fundamental parameter of the Antarctic ice sheet, ice sheet thickness is significant for dynamic ice sheet modeling of mass balance and sea level changes (Budd et al., 1991; Gogineni et al., 2001; Bamber et al., 2001; Hanna et al., 2013). Additionally, seismic waves become more complex when traveling through an ice sheet with thickness ranging in hundreds to thousands of meters thick. Thus, accurate ice sheet thickness is a critical metric for recognizing and denoising seismic multiples trapped inside the ice sheet when imaging crustal and mantle structures below the ice sheet (Lawrence et al., 2006; Hansen et al., 2009, 2010). Therefore, better ice sheet thickness and structures can also improve the study of the geological structure underneath the ice sheet in Antarctica.

Given the importance of Antarctic ice sheet structures, many geophysical methods, such as drilling, gravity modelling, radio echo sounding (RES), and active seismic approaches including reflection and refraction, have been used in local or regional scale ice sheet thickness investigations since the 1950s (Bentley and Ostenso, 1961; Bentley, 1964; Evans and Robin, 1966; Evans and Smith, 1969; Robin, 1972; Drewry et al., 1982; Cui et al., 2016). By studying gravitational anomalies in the ice sheet, gravimetric measurements provide an indirect way to infer the average ice thickness over a region. Active seismic and RES methods can determine the ice thickness at a much smaller area by converting the echo time of seismic and electromagnetic waves into an estimation of ice thickness. Among these methods, the active seismic and RES methods are the most widely used techniques for ice thickness measurements due to their relatively high accuracy and better spatial resolution, while gravity modelling is used as a complementary way in areas where lack direct ice thickness measurements. Using these methods (with the dominance of the RES method), abundant ice thickness data were collected over the past few decades. Compiled and gridded, these increasing data volumes were used to construct the Bedmap1 and Bedmap2 databases at a resolution of 5 km and 1km, respectively (Lythe et al., 2001; Fretwell et al., 2013). However, traditional methods for estimating ice thickness still have limitations. For example, the accuracy of the gravity method is relatively low because of its intrinsically low sensitivity of a gravimeter to the gravitational anomalies related to the ice sheet-bedrock interface. In the case of the active seismic and RES methods, they require considerable economic and logistical support to collect the data. With the rapid growth of cryo-seismology in the last one to two decades, many passive seismic methods have been applied to cryospheric research (Podolskiy and Walter, 2016; Aster and Winberry, 2017). Given that passive seismic methods can mitigate logistical problem and ~~is-are~~ relatively cost-efficient (Zhan et al., ~~2013~~2014; Picotti et al., 2017), it is therefore of interest to explore the feasibility of passive seismic methods to contribute additional and/or better constraints to the ice sheet structure.

Teleseismic P-wave receiver functions (PRF), as a generally used passive seismic method to determine crustal and mantle discontinuities, is also sensitive to the ice-bedrock interface and the seismic properties of ice sheets. Hansen (2010) successfully modelled ice sheet thickness beneath several stations in East Antarctica using PRF. Wittlinger and Farra (2012, 2015) investigated the anisotropy of the polar ice sheet by modelling the P-to-S



66 wave conversion with the negative PRF amplitude. Yan (2017) confirmed that the ice thickness results derived  
67 from PRF are consistent with the Bedmap2 ice thickness database. However, large numbers of teleseismic  
68 events are needed to perform PRF; it usually takes at least a one-year period of data collection, thus greatly  
69 limiting the application of the PRF method in harsh environments such as those found in Antarctica.

70 In order to improve the efficiency of ice thickness investigation, we selected the horizontal-to-vertical spectral  
71 ratio (H/V) method to determine ice thickness. As a passive and non-invasive seismic method, the H/V  
72 technique has been extensively used in seismic exploration as a tool to detect sediment thickness (Konno and  
73 Ohmachi, 1998; Ibs-von Seht and Wohlenberg, 1999; Bonnefoy-Claudet et al., 2006; ~~Bao et al., 2017~~).  
74 Considering that the sediments and ice sheet layer are both low shear-wave velocity ( $V_s$ ) layers atop the high  
75 velocity bedrock, the H/V method should be suitable for determining ice sheet thickness.

76 Lévêque (2010) applied the H/V method to four stations in the Dome C region of Antarctica for inferring the  
77 uppermost snow layer thickness and its corresponding ice properties to a few meters depth. Picotti (2017)  
78 recently adopted the H/V method to detect glacial ice thickness ranging from a few tens of meters to ~800 m in  
79 Italy, Switzerland, and West Antarctica. The H/V method has been validated for its reliability to measure glacial  
80 thickness comparing with the radio-echo sounding, geoelectric, and active seismic methods implemented at or  
81 near the same study sites. The great advantage of the H/V method over other approaches is that there is no need  
82 to record earthquakes or active sources, since it utilizes seismic ambient noise. Moreover, the H/V method  
83 requires only a few tens of minutes of seismic ambient noise recordings at single portable three-component  
84 seismometers. This greatly enhances efficiency and reduces cost and logistical support requirements.

85 Shear-wave velocity is an important parameter that controls the shear-wave impedance contrast (product of  
86 density and shear-wave velocity) at the interface between the upper and the lower layers. Since the shear-wave  
87 velocity of an ice sheet is  $\sim 1900 \text{ m s}^{-1}$ , and generally much higher than a snow layer ( $\sim 700 \text{ m s}^{-1}$ ), therefore the  
88 impedance contrast of the ice sheet-bedrock half-space is not as high as that of the snow-ice sheet layer.  
89 Moreover, the H/V spectrum may be more complicated than that of a glacier or snow layer given the complex  
90 subglacial environment since there might be subglacial lakes and sedimentary layers. In addition, the internal ice  
91 structure might affect the H/V spectrum given the variations in seismic velocities induced by changes in density,  
92 and temperature, as well as the ice crystal size and orientation of an ice sheet. Whether the H/V method can be  
93 used to estimate the ice sheet thickness or not remains an open question. Although the H/V method has been  
94 successfully applied to study snow and shallow glacial thickness (Lévêque et al., 2010; Picotti et al., 2017), to  
95 our knowledge, the H/V method has not been performed to estimate Antarctic ice sheet thickness yet. In this  
96 study, we present estimated ice thickness results from 65 stations with a typical coverage deployed on the  
97 Antarctic ice sheet to verify the feasibility of using the H/V method as an effective way to measure ice thickness.

99 **2.1 Data**

100 Over the past two decades, several temporary seismic arrays have been deployed in Antarctica, including the  
101 Transantarctic Mountains Seismic Experiment (TAMSEIS, 2000—2003) (Lawrence et al., 2006), the  
102 Gamburtsev Antarctic Mountains Seismic Experiment (GAMSEIS, 2007—2012) (Hansen et al., 2010), and the  
103 Polar Earth Observing Network/Antarctic Network (POLENET/ANET, 2007—2016) (Chaput et al., 2014).  
104 Despite their relatively sparse distribution compared to many dense seismic arrays on other continents, these  
105 three arrays together effectively cover East, and West Antarctica as well as the Transantarctic Mountain region  
106 (Fig. 1). In these three arrays, all stations are equipped with the Güralp CMG-3T or Nanometrics T-240  
107 broadband sensors with a sampling rate of 25 Hz or 40 Hz. Most stations are buried 1—2 meters below the  
108 surface snow to guarantee data quality (mainly to ensure good coupling and to dampen wind noise) (Anthony et  
109 al., 2015). Equipped with solar panels and rechargeable batteries, the GAMSEIS and POLENET/ANET stations  
110 work continuously year round except the TAMSEIS, and provide abundant seismic ambient noise waveforms  
111 for the H/V processing. To investigate the effectiveness of the H/V method for ice thickness measurements and  
112 the proper time length for H/V processing, we selected seismic ambient noise records lasting about five days (an  
113 example of such raw ambient noise record is shown in supplementary Fig. S1), which is much longer than that  
114 used in usual H/V data processing (only a few minutes' records for sedimentary investigations with tens to  
115 hundreds of meters thick). In total, 65 stations deployed on the Antarctic ice sheet were used in this study.

116 **2.2 Methods**

117 The single-station H/V method, extensively used in sediment structure detection, acquires reliable sediment  
118 thickness and shear-wave velocities (Nogoshi and Igarashi, 1971; Nakamura, 1989). In this method, seismic  
119 ambient noise data are collected by a three component seismometer and the ratio between the horizontal (H) and  
120 vertical (V) Fourier spectra are calculated. The principle of the technique can be understood by assuming a low  
121 velocity sedimentary layer overlying a high velocity bedrock half-space. Due to the sharp impedance contrast at  
122 the interface between the two layers, the shear-wave energy within the sedimentary layer produces a prominent  
123 peak that can be observed in the H/V spectrum.

124 During the relatively long history of the H/V method, extensive field experiments and numerical simulations  
125 have been carried out to confirm the correspondence between the shear-wave resonance frequency and the H/V  
126 peak frequency. Initially Nakamura (1989) proposed that the peak frequency corresponds to the transfer function  
127 for vertically incident SH waves (a polarized shear-wave that is generated when an incident shear-wave enters in  
128 a heterogeneous medium). Using numerical simulations of ambient noise in a soil layer overlying a hard bedrock,  
129 Lachetl and Bard (1994) first showed that the peak frequency is very close to the shear-wave resonance  
130 frequency. This statement—correspondence between the H/V peak frequency and the shear-wave resonance

131 ~~frequency~~ was later confirmed by Bard (1998), Ibs-von Seht and Wohlenberg (1999), and reasserted by  
132 Nakamura (2008) ~~after modification of the previous assumption. The peak in the H/V spectrum may also be~~  
133 ~~followed by a trough. Besides the peak in the H/V spectrum, a trough followed the peak may also appear in the~~  
134 ~~spectrum.~~ Konno and Ohmachi (1998) found such feature in the H/V spectrum in the case of a soft sediment  
135 layer atop a hard bedrock. ~~As indicated by~~ As pointed out by Tuan (2011),~~s~~ the appearance of a trough  
136 probably suggests the ~~aboveoverlying~~ layer has higher Poisson's ratio ~~(or impedance contrast) than that of the~~  
137 ~~underlying layer or the impedance contrast is high enough between the bedrock and the particular overlying~~  
138 ~~layer.~~ Despite the H/V peak frequency is commonly accepted as a proxy of the resonance frequency of a  
139 particular layer, no strong evidences support that the peak amplitude indicates the amplification factor of the  
140 site and there are some controversies about the nature of the ambient noise wavefield and its sources  
141 (Sánchez-Sesma et al., 2011). During the past few decades, two research branches were formed to interpret the  
142 ambient noise wavefield: Rayleigh wave ellipticity (Fäh et al., 2001; Wathelet et al., 2004) and the full  
143 wavefield assumptions including distributed surface sources (DSS, Lunedei and Albarello, 2009, 2010) and  
144 diffuse field assumption (DFA, Shapiro and Campillo, 2004; Sánchez-Sesma and Campillo, 2006;  
145 Sánchez-Sesma et al., 2011; García-Jerez et al., 2013, 2016).

146 To calculate the H/V spectrum, a specialized GEOPSY program was developed by the European SESAME  
147 team, and widely used to investigate the sediment structures (Bard and SESAME team, 2005). Then an  
148 approximation equation or H/V spectrum inversion approach can be used to derive the sedimentary layer  
149 thickness with the H/V spectrum.

150 Under the assumption of one-dimensional velocity subsurface conditions, in cases of homogenous and  
151 isotropic sedimentary layers over a homogenous half-space, the observed peak frequency equals the  
152 fundamental resonancet frequency of the sedimentary layer. Thus, the resonance frequency of the low velocity  
153 layer is closely related to its thickness  $h$  through the following relationship (Ibs-von Seht and Wohlenberg, 1999;  
154 Parolai et al., 2002; Picotti et al., 2017; Civico et al., 2017):

$$155 \quad h = \frac{Vs}{4f_0} \quad (1)$$

156 ~~Where-where~~  $Vs$  is the average shear-wave velocity of the sedimentary layer, and  $f_0$  is the observed peak  
157 frequency. Provided that a correct estimate of the average shear-wave velocity of the sedimentary layer is  
158 available, its thickness can be ~~roughly-approximately~~ estimated.

159 Complicated sedimentary internal structures, including anisotropy and low velocity layers beneath stations,  
160 will affect the H/V spectrum and consequently violate the assumptions of Eq. (1). Therefore, when inferring  
161 complex subsurface structures, an inversion of the full H/V spectrum can be used to explain more accurately the  
162 observed H/V spectrum. Based on different assumptions (including Rayleigh wave ellipticity, DSS, and DFA)  
163 for the interpretation of ambient noise wavefield composition, several inversion schemes have been proposed  
164 and successfully applied to study sedimentary structures (Fäh et al., 2003; Arai and Tokimatsu, 2004; Herak,

2008; Lunedei and Albarello, 2009; Sánchez-Sesma et al., 2011). These assumptions differentiate themselves in the scheme of forward calculation of the H/V spectrum. In this study, a more recently developed H/V spectrum forward calculation and inversion method based on the DFA was employed (García-Jerez et al., 2016). The DFA was proposed on the base of the recently stated connection between the diffuse fields and the Green's function which arises from the ambient noise interferometry theory. Under this assumption, the average energy densitiespectral power ( $P(\omega)$ ) of a diffuse field along each Cartesian axis are proportional to the imaginary part of Green's tensor components at an arbitrary point  $x$  and circular frequency  $\omega$  (i.e.  $P_i(\omega) \propto \text{Im}[G_{ii}(x; x; \omega)]$ ,  $i = 1, 2, 3$ , where 1 and 2 stand for the horizontal directions and 3 denotes the vertical direction; terms with 1 and 2 in fact are equal). Thus, the H/V spectral ratio is given as:

$$HV(x; \omega) = \sqrt{\frac{P_1(x; \omega) + P_2(x; \omega)}{P_3(x; \omega)}} = \sqrt{\frac{2 \text{Im}[G_{11}(x; x; \omega)]}{\text{Im}[G_{33}(x; x; \omega)]}} \quad (2)$$

~~$$HV(x; \omega) = \sqrt{\frac{P_1(x; \omega) + P_2(x; \omega)}{P_3(x; \omega)}} = \sqrt{\frac{2 \text{Im}[G_{11}(x; x; \omega)]}{\text{Im}[G_{33}(x; x; \omega)]}}$$~~

(2)

In a horizontally layered structure, the contribution of both the surface wave and the body wave to the  $\text{Im}[G_{ii}(x; x; \omega)]$  (on the right-hand side of Eq. (2)) can be computed with provided medium properties including primary- and shear-wave velocities. Based on a layered isotropic structure with the known primary and shear wave velocities, mass density and thickness of each layer, the contribution of surface wave and body wave can be separately computed. The detailed formulations are not stated here as they are very complicated and on account of space limitation, but readers with interest can refer to Sánchez-Sesma (2011), García-Jerez (2016), and Lunedei and Malischewsky (2015). Thus, the Eq. (2) allows for the H/V spectrum inversion as it links the real measurements and the theoretical calculation of an H/V spectrum. In the H/V spectrum inversion procedure, model spaces are set for parameters including primary- and shear-wave velocities, mass density, and thickness of each layer. The sedimentary structures can be determined when the lowest misfit between the observed and forward calculated H/V spectrum is obtained using inversion algorithms such as Monte Carlo sampling and simulated annealing.

$$E(m) = \frac{\sum_j (HV^{obs} - HV_j^{theo}(m))^2}{\sigma^2} \quad (3)$$

Where  $E(m)$  is the lowest value of the misfit in the  $j$  iterations, and  $m$  represents a model that is comprised of primary- and shear-wave velocities, mass density, and thickness of each layer in each iteration.

193  $HV^{obs}$ ,  $HV_j^{theo}(m)$  are the observed and the  $j$ -th forward calculated H/V spectrum, and  $\sigma$  is the standard  
194 deviation associated with the  $HV^{obs}$ , respectively.

195 The H/V method has been successfully applied in studies of sedimentary structures, ~~such as studies of~~  
196 ~~thickness and shear wave velocities~~ (Ibs-von Seht and Wohlenberg, 1999; Langston and Horton, 2014; Civico  
197 et al., 2017; ~~Bao et al., 2017~~). However, applications in ice environments are rare. L  v  que (2010) studied the  
198 snow layer thickness and the ice properties beneath four stations in Dome C region of Antarctica using the H/V  
199 method. Picotti (2017) measured ice thickness ranging from tens of meters to 800 m of six glaciers in Italy,  
200 Switzerland and West Antarctica. However, the impedance contrast between the ice sheet layer and the  
201 overlying bedrock is not as high as that of sedimentary-bedrock and snow-ice layers. Moreover, the complex  
202 subglacial environment and internal ice structure create other technical obstacles. Thus, there have been no  
203 investigations of ice sheet thickness incorporating the H/V method for measurements or estimations.

204 In this study, the H/V spectra of 65 stations deployed on ice were processed by using the GEOPSY software.  
205 Under the general assumption that the seismic properties are stable throughout the whole ice column, we  
206 calculated the ice thickness using Eq. (1) as in most seismological applications to approximate the ice sheet as a  
207 homogeneous layer. Meanwhile, a non-linear H/V spectrum inversion method developed by Garc  a-Jerez (2016)  
208 was adopted to constrain the observed H/V spectrum to infer the ice structure, comprised of shear-wave velocity  
209 and thickness.

210 During H/V spectrum acquisition using the GEOPSY software, we remove the transient signals (earthquakes)  
211 from noise records with the STA/LTA technique and divide the records into 600 s length windows with an  
212 overlap of 5 %. Time series were tapered with a 5 % cosine function, and the FFT was calculated for each  
213 component. The spectra were smoothed with a Hanning window in a bandwidth of 0.1—2 Hz on a logarithmic  
214 frequency scale. The spectra of the two horizontal components (NS and EW) were merged to one horizontal  
215 component spectrum by calculating their geometric mean. The spectral ratios and corresponding standard  
216 deviation estimates between the horizontal component and the vertical component were calculated.

217 Having acquired the resonance frequency of the ice sheet, we adopted Eq. (1) with a uniform average  
218 shear-wave velocity—1900 m s<sup>-1</sup> of the ice layer to calculate the ice thickness. This velocity used here is  
219 reasonable given that it is in the general range of ice Vs determined by seismic experiments (Kim et al., 2010).  
220 Moreover, this velocity has also been widely used in previous studies (Hansen et al., 2010; Wittlinger and Farra,  
221 2012; Ramirez et al., 2016). Keeping the velocities set, the ice thickness at each station was calculated using Eq.  
222 (1).

223 In the H/V spectrum inversion procedures, Bedmap2 ice thicknesses were used as references to build the  
224 initial models, as along with the related seismic elastic parameters (Fig. 2, Wittlinger and Farra, 2012; Ramirez  
225 et al., 2016). We adopted two different models assuming the ice sheet is homogenous and inner ice stratified;  
226 respectively, as shown in Fig. 2 to perform H/V spectrum inversion. Model A is a simple homogeneous and

227 isotropic ice structure with an ice layer overlying the half-space. In this model, the ice thickness varies from 0.7  
228 to 1.3 times the Bedmap2 ice thickness for each station. Model B is constructed following Wittlinger [and Farra](#)  
229 (2012, 2015) as a two-layer ice structure in which a low shear-wave velocity lies in the lower ice layer. In this  
230 model, the thickness of the upper ice layer and the lower ice layer were set to occupy 60—75 and 25—40 percent  
231 of the Bedmap2 thickness, respectively. Using the non-linear Monte Carlo method (García-Jerez et al., 2016),  
232 we retrieved the optimum solutions for model A and B. These two solutions were best fitted to the observed H/V  
233 spectrum.

234 It usually takes a few minutes to about half an hour to collect seismic ambient noise waveforms in the  
235 investigations of sedimentary layers with thickness ranging from several tens to hundreds of meters. However,  
236 there is no experiences for the time length of recording seismic ambient noise in the Antarctic ice sheet with  
237 several kilometers thick. It is necessary to apply the H/V method with a much shorter recording time for seismic  
238 ambient noise, considering the harsh environment and logistical support difficulties in Antarctica. Therefore, we  
239 investigated the feasibility and reliability of H/V method by testing a range of noise record lengths; eight hour,  
240 four hour, two hour, and one hour intervals were tested. The processing strategies remained the same as in H/V  
241 spectrum acquisition except the window length was changed to 200 s when calculating the H/V spectrum using  
242 different length noise records.

### 243 3 Results

244 In this study, the H/V spectra of 65 stations were obtained. Figure 3 displays the H/V spectra of nine stations  
245 selected from three arrays. These examples are representative of all the results, and the remaining spectra are  
246 presented in the supplementary Fig. S2. It is clearly shown that in almost all H/V spectra there were two or three  
247 clear peaks in the frequency band. Generally, the largest amplitude appears at the first peak located around 0.2  
248 Hz or below, and the second and the third peaks with lower amplitudes are located at  $\sim 0.5$  and  $\sim 0.8$  Hz,  
249 respectively. Following the general interpretation principles for H/V spectra (Bard and SESAME team, 2005),  
250 the peak frequency denoting the largest amplitude should be the resonance frequency of the ice sheet layer, while  
251 the peaks appearing with lower amplitudes at higher frequencies may indicate the shallower impedance contrast  
252 layers. The reasonableness of considering the first peak frequency with the largest amplitude as the resonance  
253 frequency of the ice sheet layer was verified through ~~rough estimation~~[approximate estimation](#) based on Eq. (1),  
254 i.e., for station E012, the Bedmap2 ice thickness at that location is 1050 m, so the resonance frequency according  
255 to Eq. (1) should be 0.452 Hz (the given  $V_s$  is  $1900 \text{ m s}^{-1}$ ), and as expected was observed ( $0.418 \pm 0.052$  Hz) in the  
256 H/V spectrum. However, there are exceptions such as station N108 displayed in Fig. [2-3](#) whose first peak  
257 ( $0.177 \pm 0.014$  Hz) amplitude is slightly lower than that of the following peak observed at higher frequency  
258 ( $1.666$  Hz). At this station however, the location of the first peak correlates with the resonance frequencies  
259 ( $0.194$  Hz) through ~~rough estimation~~[approximate estimation](#). In addition, there are some stations that have no  
260 peak frequencies correlating with the ice sheet thickness, despite the existence of peak frequency with strong

261 amplitude in the frequency band. Station ST07 seen in Fig. 3 is such a case, whose fundamental resonance  
262 frequency as calculated by Eq. (1) should be 0.191 Hz (its Bedmap2 ice thickness is 2490 m). Nevertheless, no  
263 clear peak around this expected frequency is observed in the H/V spectrum. We therefore can group the results  
264 into three categories:

- 265 1) 42 stations with first peaks denoting the largest amplitude in the observed spectrum related to the ice sheet  
266 resonance frequency, like the E012, E018, GM02, N148, P071, ST01, ST02 stations in Fig. 3.
- 267 2) 18 stations with first peaks with slightly lower amplitude but also related to the ice sheet resonance  
268 frequency such as station N108.
- 269 3) Five stations without peaks correlating to the resonance frequency, such as station ST07.

270 Figure 4 shows the H/V spectra of stations along four profiles, together with the ice sheet and bedrock  
271 elevation extracted from Bedmap2 database for each station. As shown in Fig. 4, although the neighboring  
272 stations are 80 km apart for profile AA', 100 km for profile BB' and DD', and 20 km for profile CC', the shape  
273 of the spectra are similar along each profile. Also, along each profile, the peaks associated with the ice thickness  
274 are clear and the locations of the peaks shift towards lower or higher frequencies cohering with the variation of  
275 the corresponding ice thickness. There are four stations (N060, ST04, ST06, ST07) along the four profiles  
276 without peak frequencies related to their corresponding ice thicknesses. This may be caused by the bad coupling  
277 of the seismometer with the ice surface or possibly a complicated subglacial environment, for example clear  
278 evidence indicates the existence of sedimentary layer beneath station N060.

279 Having identified resonance ~~frequency-frequencies~~ of the ice sheet, we calculated the ice thickness using Eq.  
280 (1) with the average shear-wave velocity—1900 m s<sup>-1</sup>. The ~~Equation (1) estimatesresults~~ together with their  
281 relative errors to the corresponding Bedmap2 ice thickness are listed in Table 1(~~hereafter the ice thickness~~  
282 ~~estimations derived from the approximation Eq. (1) and H/V spectrum inversions using model A and model B~~  
283 ~~are defined as Equation (1), DFA + Model A, and DFA + Model B estimates, respectively~~). We projected the  
284 ~~Equation (1) estimatesealeulated ice thickness~~ and the reference Bedmap2 ice thickness for stations along the  
285 four profiles in the upper elevation panels in Fig. 4. It is clear that the ~~Equation (1) estimatesealeulated ice~~  
286 ~~thickness~~ for some stations along the four profiles are close to the reference ice thickness like the E012, P071,  
287 and ST01 stations, while there are large deviations at some stations such as E018, N148, and ST02. It should be  
288 noted that the ice thickness obtained from the H/V method reflects the average ice sheet thickness beneath each  
289 station in the scale of seismic wavelength (i.e. for a peak at frequency 0.2—1 Hz and seismic wavelength of ~2.0  
290 km, the spatial resolution (or footprint) is about 2—10 km).

291 The optimum shear-wave velocity models derived from H/V spectrum inversion are presented in Fig. 5 and  
292 supplementary Fig. S3. The observed H/V spectrum together with the synthetic H/V spectra using the two  
293 optimum shear-wave velocity models are plotted in Fig. 6 and shown in supplementary Fig. S4. As Fig. 6 and the  
294 supplementary Fig. S4 shows, the synthetic H/V spectra of the optimum inversion results for model A and model  
295 B at almost all stations, both fit the observed H/V spectra in peak frequency and spectrum shape. However, the

296 ~~DFA + Model A estimates the inversion ice thickness from model A~~ deviates substantially from the Bedmap2  
297 thickness at most stations (such as N108, N148, GM02 and ST02 in Fig. 5), and the difference extends 1 km for  
298 some stations (Fig. 7). By contrast, the ~~DFA + Model B estimates inversion thickness from model B~~ is  
299 consistent with the Bedmap2 thickness as the differences between them are mostly within 200 m. The overall  
300 ~~DFA + Model B estimates inversion ice thicknesses from model B~~ are listed in Table 1, as well as the relative  
301 errors to the corresponding Bedmap2 ice thickness. We also projected ~~the DFA + Model B estimates the~~  
302 ~~inversion thickness~~ for stations along the four profiles in the elevation panels seen in Fig. 4. This figure depicts a  
303 good consistency between the ~~DFA + Model B estimates inversion~~ and the reference ice thickness as the ice  
304 thickness at ~~26-27~~ stations and 46 stations out of the 48 stations along the profiles are within 10 % and 15 %  
305 threshold of the Bedmap2 ice thickness.

306 The results of four different length seismic ambient noise records (1 h, 2 h, 4 h, 8 h) used to obtain H/V  
307 spectrum are displayed in Fig. 8 (and in supplementary Fig. S5). These plots show that the shape of the spectra of  
308 the four tested record lengths are similar to the shape determined using a record five days long. The peak  
309 frequencies of the four different length records are all within the margin of error for the peak frequency as  
310 determined with the record five days long. Besides, we found that the longer the ambient noise record, the more  
311 stable the peak frequency is as there are slight shifts in the peak frequency when determined with 1 h records.  
312 This feature is obvious for stations with thin ice (less than 2 km) such as those from stations E018 (Fig. 8), E014,  
313 E020, E024, and E028 (shown in supplementary Fig. S5). The quality of the H/V spectrum obtained from one  
314 hour long record for stations with thick ice (over 2 km) however, is generally ~~in-consistence-consistent~~  
315 determined with the record five days long. This consistency can also be found for all stations when the length of  
316 noise record exceeds two hours.

#### 317 4 Discussion

318 Bedmap2 ice thickness ~~were was~~ used as reference to verify the ~~ice thickness derived from Eq. (1) and H/V~~  
319 ~~spectrum inversion~~ Equation (1), DFA + Model A, and DFA + Model B estimates since we lacked actual ice  
320 thickness as obtained from the more direct and accurate ice-core drilling, RES and active seismic methods at or  
321 near each study site. Because of various factors contributing to the uncertainty in the Bedmap2 database such as  
322 data coverage, basal roughness, and ice thickness measurement and gridding error, however, the Bedmap2 ice  
323 thickness is not exactly accurate with uncertainty varying from site to site. We obtained the uncertainty of the  
324 Bedmap2 ice thickness at each station from the grids of ice thickness uncertainty (Fretwell et al., 2013, also, the  
325 uncertainty at our study sites can be roughly seen in supplementary Fig. S6). A close examination of the  
326 uncertainty of the Bedmap2 ice thickness reveals that the uncertainty at 52 stations ranges from 59 m to about  
327 200 m, and the uncertainty at 57 stations is below 300 m. As the accuracy of the H/V method is at the same scale  
328 with the uncertainty of the Bedmap2 ice thickness at the 57 stations, the Bedmap2 ice thicknesses are adequate to



329 verify the results derived from the H/V method. The remaining three stations including ST09, ST13, and ST14  
330 are excluded for validation as the uncertainty of the reference ice thickness at these stations reaches 1000 m.

331 A comparison of the ~~inversion ice thickness from DFA + Model B estimates~~ Model B and Bedmap2 database  
332 reveals that the differences in ice thickness at all the 57 stations are less than 400 m; there are ~~33-34~~ stations  
333 whose differences are within 200 m and ~~47-48~~ stations within 300 m; the maximum difference was ~~370-360~~ m at  
334 stations GM06 and N215ST03. The relative errors of the ~~DFA + Model B estimates~~ inversion ice thickness to the  
335 corresponding Bedmap2 thickness of ~~22-23~~ stations, ~~35-36~~ stations, and 58 stations are within 5 %, 10 %, and  
336 15 % threshold, respectively. Given that the Bedmap2 ice thickness are associated with certain uncertainties at  
337 each station (i.e. the relative errors of the uncertainty to the Bedmap2 ice thickness are within 10 % at 49 stations)  
338 (Fretwell et al., 2013). In this sense, we conclude that the ~~DFA + Model B estimates~~ inversion ice thickness has  
339 comparable accuracy to the Bedmap2 ice thickness at the study sites.

340 Based on the homogenous ice sheet layer assumption, most of the ~~ice thickness estimations derived from Eq.~~  
341 ~~(1)-Equation (1) estimates~~ are not compatible with Bedmap2 ice thickness (Fig. 4 and Fig. 7), as the differences  
342 at ~~26-25~~ stations can extend 400 m and at 10 stations are over 600 m; the maximum difference reaches 910 m at  
343 station N036. Moreover, most of the ~~DFA + Model A estimates~~ inversion ice thickness results based on the  
344 homogenous ice structure of model A also largely deviated from the reference Bedmap2 thickness (Fig. 7 and  
345 supplementary Fig. S3). These large deviations cannot be attributed to the uncertainty in the reference Bedmap2  
346 ice thickness since they made minor contributions to the large differences.

347 The ~~inversion DFA + Model B estimates~~ ice thickness from model B, however ~~were~~ are in good consistence  
348 highly consistent with the Bedmap2 database (Table 1). A close examination of the DFA + Model B  
349 estimates ~~the inversion thickness from model B~~ shows that it refined the Equation (1) estimates ~~rough estimation~~  
350 results at 47 stations ~~as calculated with Eq. (1)~~ to varying degrees. As at stations E012 and N036, the Equation (1)  
351 estimates ~~calculated ice thicknesses using Eq. (1)~~ deviate from Bedmap2 at 90 m and 910 m, while the DFA +  
352 Model B estimates ~~the inversion ice thickness from model B~~ refines the gaps to 20 m and 320 m.

353 We compared our results with those found in Wittlinger and Farra (2012). Using the PRF method and a grid  
354 search stacking technique, they found that the Antarctic ice is stratified, possibly due to the preferred orientation  
355 of ice crystals and fine layering of soft and hard ice layers under pressure. In Fig.9, we present the ice ~~thickness~~  
356 sheet structure ~~results~~ for 12 stations common to both studies. It is clear that the interface separating the upper  
357 and the lower ice sheet layers determined using the H/V method and the PRF method, is consistent for almost all  
358 stations.

359 The agreement of two-layer ice sheet thickness with the Bedmap2 database, and the consistency of our results  
360 to Wittlinger and Farra (2012)'s results, as well as the large deviation of Equation (1) estimates ~~ice thickness~~  
361 estimated using Eq. (1) and DFA + Model A estimates ~~model A~~ jointly support the thesis that the two-layered ice  
362 sheet models are more reasonable than an homogeneous ice sheet layer assumption. Moreover, the Equation (1)  
363 estimates ~~the ice thickness~~ of 28 stations ~~derived from Eq. (1)~~ were close to the reference Bedmap2 database.

364 This consistency, however, does not strongly support the homogenous ice sheet layer assumption as it can be  
365 attributed to the fact that the  $V_s$  values adopted in ~~rough estimation~~ approximate estimation was coincidental  
366 with the average velocity of the two-layer  $V_s$  models.

367 The examples presented in this work clearly show that the H/V method with seismic ambient noise can be  
368 effectively used to measure ice sheet thickness. However, there are also some limitations that may affect the  
369 results. Shear-wave velocity ( $V_s$ ), as the key parameter for H/V spectrum inversion and ~~rough~~  
370 ~~estimation~~ approximate estimation using Eq. (1), will significantly affect the effectiveness and uncertainty of the  
371 H/V method. We can see from Fig. 6 that the synthetic H/V spectra from the optimum  $V_s$  profiles of model A  
372 and model B for the N108, GM02 and N148 stations (~~Fig. 5~~), match the observed H/V spectrum. The DFA +  
373 Model A estimates and the DFA + Model B estimates ~~inversion ice thickness from model A and model B~~ at these  
374 stations however, are remarkably different as the DFA + Model B estimates ~~results from model B~~ are more  
375 closely match the reference Bedmap2 ice thickness than the DFA + Model A estimates ~~those from model A~~ (Fig.  
376 5). Also evident in these results is a directly proportional relationship between ice thickness and the  $V_s$  as  
377 expected from Eq. (1) in ~~rough estimation~~ approximate estimation. Given a  $\sim 5$  percent variation in the average  
378 shear-wave speed of the ice layer, then ice sheet thickness estimation will result in a similar variation such as 150  
379 m for a station with 3 km thickness. Accurate known  $V_s$  profiles are therefore prerequisites when obtaining  
380 reliable H/V spectrum inversion results, as well as for ~~rough estimations~~ approximate estimations using Eq. (1).

381 It is evident that the longer the noise record, the more stable the observed peak frequency is as the sources of  
382 the seismic ambient noise are more evenly distributed, spatially and temporally. This is significant for stations  
383 with thin ice primarily due to the fact that thin ice sheet layers are excited by high-frequency waves such as  
384 winds and other sources (Picotti et al., 2017). Thus, a longer ambient noise record can improve the stability of  
385 the H/V spectrum. In our study, we found that the quality of the H/V spectrum is generally better for thick ice  
386 sheet layers than for thin ice sheet such as stations E012, E018, E024, E026, and E028 with relatively smaller ice  
387 thicknesses than other stations. The H/V spectra for these stations exhibited less stability when the lengths of  
388 noise records decreased (Fig. 8 and supplementary Fig. S5). Their peak frequencies obtained from a one hour  
389 long record slightly deviate from the peak frequency determined with a five day record. These deviations  
390 consequently could lead to uncertainties in ice thickness estimation. While for stations with thick ice, both the  
391 shape and the peak frequency determined using a one hour long record are generally consistent with those  
392 obtained from a five day long record. Given that the variation of ice thickness at the study sites (from 600 m to  
393 about 4 km), generally covers the range of the whole Antarctic ice sheet thickness, we would like to suggest a  
394 uniform record length of two hours in H/V method application in Antarctica, in terms of stability and efficiency.  
395

## 5 Conclusions

~~Given the vital role that ice sheet thickness plays in ice mass balance and sea level changes studies, many methods have been used to estimate ice sheet thickness, obtaining abundant results. However, new methods should be explored to enrich the database considering the vast area of the Antarctic ice sheet and to provide additional constraints to the ice sheet structure from other perspectives.~~

~~In this study,~~ The H/V method is proposed as a reliable, efficient method to investigate the Antarctic ice sheet thickness. The H/V method is effective for identifying the fundamental resonant frequency correlating with the ice sheet thickness. In this approach, the ambient noise recording length can be as short as 2 hours, reducing costs and increasing efficiency. Equation (1) can retrieve a fast and ~~rough estimation~~ approximate estimation of the ice thickness but should be used with care since the shear-wave velocity varies at different sites. H/V spectrum inversion, however, unlike estimation with Eq. (1), is robust and can obtain reliable ice thickness results with given seismic properties. Moreover, the H/V spectrum inversion ice sheet thickness results are consistent with the reference Bedmap2 database. Our results also support the argument that the Antarctic ice sheet has a two-layer structure. The H/V method is an excellent approach that provides new and independent ice sheet thickness estimations. What makes this new approach most attractive are the ease and economy of seismic ambient noise waveforms collection when deploying a single seismometer for short time intervals. Finally, we hope that specific seismic experiments can obtain more accurate shear-wave velocity profiles in the ice sheet, thus making better constraints for H/V method results.

Supplementary materials include:

Figure S1, S2, S3, S4, S5, S6 in pdf format

*Competing interests.* The authors declare that they have no conflict of interest.

## Acknowledgement

We thank the editor, Kenny Matsuoka, and two reviewers, Andreas Köhler and Adam Booth for their critical and helpful comments and suggestions that greatly improved the manuscript. We thank Sidao Ni for helpful discussion on the manuscript. This work was supported by the State Key Program of National Natural Science of China under Grant 41531069, the Chinese Polar Environment Comprehensive Investigation and Assessment Programs under Grant CHINARE2017-02-03, and the Special Funds for Basic Scientific Research of

Universities under Grant 2015644020201. Seismic data are obtained from the Incorporated Research Institutions for Seismology (IRIS). Figures in this study were plotted using Generic Mapping Tools (GMT).

## References:

- Anthony, R. E., Aster, R. C., Wiens, D., Nyblade, A., Anandkrishnan, S., Huerta, A., Winberry, J. P., Wilson, T., and Rowe, C.: The seismic noise environment of Antarctica. *Seismological Research Letters*, 86(1), 89–100, 2015.
- Arai, H., and Tokimatsu, K.: S-wave velocity profiling by inversion of microtremor H/V spectrum. *Bulletin of the Seismological Society of America* 94.1: 53–63, 2004.
- Aster, R. C., and Winberry, J. P.: *Glacial Seismology*. Reports on Progress in Physics, 1–67, 2017.
- Bamber, J. L., Layberry, R. L., and Gogineni, S. P.: A new ice thickness and bed data set for the Greenland ice sheet: 1. Measurement, data reduction, and errors. *Journal of Geophysical Research: Atmospheres*, 106(D24): 33773–33780, 2001.
- ~~Bao, F., Li, Z. W., Zhao, J. Z., Ren, J., and Tian, B. F.: Shallow crustal structure of the Tangshan fault belt unveiled by dense seismic profile and H/V spectral ratio method. *Engineering Geology*, under review, 2017.~~
- Bard, P. Y.: Microtremor measurements: a tool for site effect estimation? In: Proceedings of the 2nd international symposium on the effects of surface geology on seismic motion, Yokohama, 1251–1279, 1998.
- Bard, P. Y., and Site Effects aSsessment using AMbient Excitations Team: Report D23.12, Guidelines for the implementation of the H/V spectral ratio technique on ambient vibrations measurements, processing and interpretation, in European Commission: Research general directorate, Project No. EVG1-CT-2000-00026, SESAME, 62 pp, 2005.
- Bentley, C., and Ostenso, N.: Glacial and Subglacial Topography of West Antarctica. *Journal of Glaciology*, 3(29), 882–911, 1961.
- Bentley, C. R.: The structure of Antarctica and its ice cover, in: *Research in Geophysics Vol. 2, Solid Earth and Interface Phenomena*, edited by: Odishaw, H., MIT Press, Cambridge, Mass., 335–389, 1964.
- Bonnefoy-Claudet, S., Cornou, C., Bard, P. Y., Cotton, F., Moczo, P., Kristek, J., and Fäh, D.: H/V ratio: a tool for site effects evaluation. Results from 1-D noise simulations. *Geophysical Journal International*, 167(2), 827–837, 2006.
- Budd, W. F.: Antarctica and global change. *Climatic Change*, 18(2-3): 271–299, 1991.
- Chaput, J., Aster, R. C., Huerta, A., Sun, X., Lloyd, A., Wiens, D., Nyblade, A., Anandkrishnan, S., Winberry, J. P., and Wilson, T.: The crustal thickness of West Antarctica. *Journal of Geophysical Research: Solid Earth*, 119(1), 378–395, 2014.

- 459 Civico, R., Sapia, V., Di Giulio, G., Villani, F., Pucci, S., Baccheschi, P., and Smedile, A.: Geometry and  
460 evolution of a fault-controlled Quaternary basin by means of TDEM and single-station ambient vibration  
461 surveys: the example of the 2009 L'Aquila earthquake area. *Journal of Geophysical Research: Solid Earth*,  
462 122(3): 2236–2259, 2017.
- 463 Cui, X. B., Sun, B., Su, X. G., and Guo, J. X.: Distribution of ice thickness and subglacial topography of the  
464 "Chinese Wall" around Kunlun Station, East Antarctica. *Applied Geophysics*, 13(1): 209, 2016.
- 465 Drewry, D. J., Jordan, S. R., and Jankowski, E.: Measured properties of the Antarctic ice sheet: surface  
466 configuration, ice thickness, volume and bedrock characteristics. *Annals of Glaciology* 3.1: 83–91, 1982.
- 467 Evans, S., and Robin, G. Q.: Glacier depth sounding from the air. *Nature*, 210:883–885, 1966.
- 468 Evans, S., and Smith, B. M. E.: A radio echo equipment for depth sounding in polar ice sheets. *Journal of*  
469 *Physics E: Scientific Instruments* 2.2: 131, 1969.
- 470 Fähr, D., Kind, F., and Giardini, D.: A theoretical investigation of average H/V ratios, *Geophys. J. Int.*, 145,  
471 535–549, 2001.
- 472 Fähr, D., Kind, F., and Giardini, D.: Inversion of local S-wave velocity structures from average H/V ratios and  
473 their use for the estimation of site-effects. *Journal of Seismology* 7, 449–467, 2003.
- 474 Fretwell, P., Pritchard, H. D., Vaughan, D. G., Bamber, J. L., Barrand, N. E., Bell, R., Bianchi, C., Bingham, R.  
475 G., Blankenship, D. D., Casassa, G., Catania, G., Callens, D., Conway, H., Cook, A. J., Corr, H. F. J.,  
476 Damaske, D., Damm, V., Ferraccioli, F., Forsberg, R., Fujita, S., Gim, Y., Gogineni, P., Griggs, J. A.,  
477 Hindmarsh, R. C. A., Holmlund, P., Holt, J. W., Jacobel, R. W., Jenkins, A., Jokat, W., Jordan, T., King, E.  
478 C., Kohler, J., Krabill, W., Riger-Kusk, M., Langley, K. A., Leitchenkov, G., Leuschen, C., Luyendyk, B.  
479 P., Matsuoka, K., Mouginot, J., Nitsche, F. O., Nogi, Y., Nost, O. A., Popov, S. V., Rignot, E., Rippin, D.  
480 M., Rivera, A., Roberts, J., Ross, N., Siegert, M. J., Smith, A. M., Steinhage, D., Studinger, M., Sun, B.,  
481 Tinto, B. K., Welch, B. C., Wilson, D., Young, D. A., Xiangbin, C., and Zirizzotti, A.: Bedmap2:  
482 improved ice bed, surface and thickness datasets for Antarctica, *The Cryosphere*, 7, 375–393,  
483 doi:10.5194/tc-7-375-2013, 2013.
- 484 García-Jerez, A., Luzón, F., Sánchez-Sesma, F. J., Lunedei, E., Albarello, D., Santoyo, M. A., and Almendros,  
485 J.: Diffuse elastic wavefield within a simple crustal model. Some consequences for low and high  
486 frequencies. *Journal of Geophysical Research: Solid Earth*, 118(10), 5577–5595, 2013.
- 487 García-Jerez, A., Piña-Flores, J., Sánchez-Sesma, F. J., Luzón, F., and Perton, M.: A computer code for forward  
488 calculation and inversion of the H/V spectral ratio under the diffuse field assumption. *Computers &*  
489 *Geosciences*, 97, 67–78, 2016.
- 490 Gogineni, S., Tammana, D., Braaten, D., Leuschen, C., Akins, T., Legarsky, J., Kanagaratnam, P., Stiles, J.,  
491 Allen, C., and Jezek, K.: Coherent radar ice thickness measurements over the Greenland ice sheet. *Journal*  
492 *of Geophysical Research: Atmospheres*, 106(D24), 33761–33772, 2001.

- 493 Hanna, E., Navarro, F. J., Pattyn, F., Domingues, C. M., Fettweis, X., Ivins, E. R., Nicholls, R. J., Ritz, C.,  
494 Smith, B., Tulaczyk, S., Whitehouse, P. L., and Zwally, H. J.: Ice-sheet mass balance and climate change.  
495 *Nature*, 498(7452), 51–59, 2013.
- 496 Hansen, S. E., Julia, J., Nyblade, A. A., Pyle, M. L., Wiens, D. A., and Anandakrishnan, S.: Using S wave  
497 receiver functions to estimate crustal structure beneath ice sheets: An application to the Transantarctic  
498 Mountains and East Antarctic craton. *Geochemistry, Geophysics, Geosystems*, 10(8), 2009.
- 499 Hansen, S. E., Nyblade, A. A., Heeszel, D. S., Wiens, D. A., Shore, P., and Kanao, M.: Crustal structure of the  
500 Gamburtsev Mountains, East Antarctica, from S-wave receiver functions and Rayleigh wave phase  
501 velocities. *Earth and Planetary Science Letters*, 300(3), 395–401, 2010.
- 502 Herak, M.: ModelHVSR-A Matlab® tool to model horizontal-to-vertical spectral ratio of ambient noise.  
503 *Computers & Geosciences* 34.11: 1514–1526, 2008.
- 504 Ibs-von Seht, M., and Wohlenberg, J.: Microtremor measurements used to map thickness of soft sediments.  
505 *Bulletin of the Seismological Society of America* 89.1: 250–259, 1999.
- 506 Kim, K. Y., Lee, J., Hong, M. H., Hong, J. K., Jin, Y. K., and Shon, H.: Seismic and radar investigations of  
507 Fourcade Glacier on King George Island, Antarctica. *Polar Research*, 29(3), 298–310, 2010.
- 508 Konno, K., and Ohmachi, T.: Ground-motion characteristics estimated from spectral ratio between horizontal  
509 and vertical components of microtremor. *Bulletin of the Seismological Society of America* 88.1: 228–241,  
510 1998.
- 511 Lachetl, C., and Bard, P. Y.: Numerical and theoretical investigations on the possibilities and limitations of  
512 Nakamura's technique. *Journal of Physics of the Earth*, 42(5), 377–397, 1994.
- 513 Langston, C. A., and Horton, S. P.: Three-dimensional seismic-velocity model for the unconsolidated  
514 Mississippi embayment sediments from H/V ambient noise measurements. *Bulletin of the Seismological  
515 Society of America*, 104(5), 2349–2358, 2014.
- 516 Lawrence, J. F., Wiens, D. A., Nyblade, A. A., Anandakrishnan, S., Shore, P. J., and Voigt, D.: Crust and upper  
517 mantle structure of the Transantarctic Mountains and surrounding regions from receiver functions, surface  
518 waves, and gravity: implications for uplift models. *Geochemistry, Geophysics, Geosystems*, 7(10), 2006.
- 519 Lévêque, J. J., Maggi, A., and Souriau, A.: Seismological constraints on ice properties at Dome C, Antarctica,  
520 from horizontal to vertical spectral ratios. *Antarctic Science* 22.05: 572–579, 2010.
- 521 Lunedei, E., and Albarello, D.: On the seismic noise wavefield in a weakly dissipative layered Earth.  
522 *Geophysical Journal International* 177, 1001–1014, 2009.
- 523 Lunedei, E., and Albarello, D.: Theoretical HVSR curves from full wavefield modelling of ambient vibrations  
524 in a weakly dissipative layered Earth. *Geophysical Journal International*, 181(2), 1093–1108, 2010.
- 525 Lunedei, E., and Malischewsky, P.: A review and some new issues on the theory of the H/V technique for  
526 ambient vibrations. *Perspectives on European Earthquake Engineering and Seismology*. Springer  
527 International Publishing, 371–394, 2015.

- 528 Lythe, M. B., Vaughan, D. G., and The BEDMAP Consortium: BEDMAP: A new ice thickness and subglacial  
529 topographic model of Antarctica. *Journal of Geophysical Research: Solid Earth*, 106(B6): 11335–11351,  
530 2001.
- 531 Nakamura, Y.: A method for dynamic characteristics estimation of subsurface using microtremor on the ground  
532 surface. *Railway Technical Research Institute, Quarterly Reports* 30.1, 1989.
- 533 Nakamura, Y.: On the H/V spectrum. In: *Proceedings of the 14th world conference on earthquake engineering*  
534 (WCEE), Beijing, 2008.
- 535 Nogoshi, M., and Igarashi, T.: On the amplitude characteristics of microtremor (part 2). *J. Seismol. Soc. Japan*  
536 24.1: 26–40, 1971.
- 537 Parolai, S., Bormann, P. and Milkereit, C.: New relationships between  $V_s$ , thickness of sediments, and  
538 resonance frequency calculated by the H/V ratio of seismic noise for the Cologne area (Germany).  
539 *Bulletin of the seismological society of America* 92.6: 2521–2527, 2002.
- 540 Picotti, S., Francese, R., Giorgi, M., Pettenati, F., and Carcione, J. M.: Estimation of glacier thicknesses and  
541 basal properties using the horizontal-to-vertical component spectral ratio (HVSR) technique from passive  
542 seismic data. *Journal of Glaciology*, 63(238), 229–248, 2017.
- 543 Podolskiy, E. A., and Walter, F.: *Cryo-seismology. Reviews of Geophysics*, 51, 2016.
- 544 Ramirez, C., Nyblade, A., Hansen, S. E., Wiens, D. A., Anandakrishnan, S., Aster, R. C., Huerta, A.D., and  
545 Wilson, T.: Crustal and upper-mantle structure beneath ice-covered regions in Antarctica from S-wave  
546 receiver functions and implications for heat flow. *Geophysical Journal International*, 204(3), 1636–1648,  
547 2016.
- 548 Robin, G. Q.: Radio-echo sounding applied to the investigation of the ice thickness and sub-ice relief of  
549 Antarctica. *Antarctic Geology and Geophysics*: 675–682, 1972.
- 550 Sánchez-Sesma, F. J., and Campillo, M.: Retrieval of the Green's function from cross correlation: the  
551 canonical elastic problem. *Bulletin of the Seismological Society of America*, 96(3), 1182–1191, 2006.
- 552 Sánchez-Sesma, F. J., Rodríguez, M., Iturrarán-Viveros, U., Luzón, F., Campillo, M., Margerin, L.,  
553 García-Jerez, A., Suarez, M., Santoyo, M. A., and Rodríguez-Castellanos, A.: A theory for microtremor  
554 H/V spectral ratio: Application for a layered medium. *Geophysical Journal International*, 186(1), 221–225,  
555 2011.
- 556 Shapiro, N. M., and Campillo, M.: Emergence of broadband Rayleigh waves from correlations of the ambient  
557 seismic noise. *Geophysical Research Letters*, 31(7), 2004.
- 558 Tuan, T. T., Scherbaum, F. and Malischewsky, P. G.: On the relationship of peaks and troughs of the ellipticity  
559 (H/V) of Rayleigh waves and the transmission response of single layer over half-space models.  
560 *Geophysical Journal International*, 184: 793–800, 2011.

- 561 Wathelet, M., Jongmans, D., and Ohrnberger, M.: Surface wave inversion using a direct search algorithm and  
562 its application to ambient vibration measurements. *Near Surface Geophysics*, 2, 211–221, 2004.
- 563 Wittlinger, G., and Farra, V.: Observation of low shear wave velocity at the base of the polar ice sheets:  
564 evidence for enhanced anisotropy. *Geophysical Journal International*, 190(1): 391–405, 2012.
- 565 Wittlinger, G., and Farra, V.: Evidence of unfrozen liquids and seismic anisotropy at the base of the polar ice  
566 sheets. *Polar Science* 9.1: 66–79, 2015.
- 567 Yan, P., Li, Z. W., Li, F., Yang, Y. D., Hao, W. F., and Zhou, L.: Antarctic ice sheet thickness derived from  
568 teleseismic receiver functions. *Chinese Journal of Geophysics (in Chinese)*, 60(10): 3780–3792, 2017.
- 569 Zhan, Z., Tsai, V. C., Jackson, J. M., and Helmberger, D.: Ambient noise correlation on the Amery Ice Shelf,  
570 east Antarctica. *Geophysical Journal International*, 196 (3):1796–802, ~~2013~~[2014](#).
- 571



Table 1 Ice thickness results obtained from this study

(Error of Equation (1) estimates listed in column 4 is obtained by averaging the thickness using the resonance frequency  $f_0$  and its corresponding standard deviation  $\sigma$  (i.e.  $\Delta h = \left( \left( \frac{V_s}{f_0} - \frac{V_s}{f_0 + \sigma} \right) + \left( \frac{V_s}{f_0 - \sigma} - \frac{V_s}{f_0} \right) \right) / 2$ ). The relative errors listed in column 5 and 7 are calculated using  $\frac{|Equation(1) - Bedmap2|}{Bedmap2} \cdot 100\%$  and  $\frac{|DFA + Model B - Bedmap2|}{Bedmap2} \cdot 100\%$  respectively (Thickness I, II are ice thickness values obtained from Eq. (1) and model B, respectively)

Station	Bedmap2 (km)	Resonance freq. (Hz)	Thickness Equation (1) (km)	Relative error	Thickness DFA+Model B (km)	Relative error
BENN	1.56	0.222±0.034	2.14±0.33	37.18%	1.73	10.90%
BYRD	2.16	0.222±0.022	2.14±0.21	0.93%	2.33	7.87%
E012	1.05	0.418±0.052	1.14±0.14	8.57%	1.03	1.90%
E014	0.66	0.914±0.085	0.52±0.05	21.21%	0.60	9.09%
E018	1.50	0.222±0.028	2.14±0.27	42.67%	1.72	14.67%
E020	1.75	0.200±0.011	2.38±0.13	36.00%	2.01	14.86%
E024	1.83	0.200±0.019	2.38±0.22	30.05%	2.09	14.21%
E026	1.40	0.215±0.028	2.2±0.29	57.14%	1.61	15.00%
E028	1.61	0.188±0.032	2.5±0.44	55.28%	1.85	14.91%
E030	2.02	0.177±0.024	2.68±0.37	32.67%	2.32	14.85%
GM01	3.10	0.155±0.018	3.07±0.36	0.97%	3.12	0.65%
GM02	2.81	0.159±0.014	2.98±0.26	6.05%	2.94	4.63%
GM03	2.52	0.159±0.018	2.98±0.33	18.25%	2.88	14.29%
GM04	2.80	0.157±0.015	3.02±0.29	7.86%	3.08	10.00%
GM05	3.47	0.146±0.020	3.26±0.45	6.05%	3.17	8.65%
GM06	3.47	0.150±0.015	3.16±0.32	8.93%	3.10	10.66%
GM07	3.03	0.148±0.012	3.21±0.26	5.94%	3.08	1.65%
JNCT	1.19	0.349±0.031	1.36±0.12	14.29%	1.26	5.88%
N020	1.71	0.222±0.021	2.14±0.21	25.15%	1.95	14.04%
N028	2.06	0.197±0.020	2.41±0.25	16.99%	2.24	8.74%
N036	2.21	0.152±0.020	3.12±0.41	41.18%	2.53	14.48%
N044	2.21	0.169±0.023	2.81±0.39	27.15%	2.51	13.57%
N052	2.39	0.152±0.022	3.12±0.45	30.54%	2.75	15.06%
N068	2.87	0.155±0.014	3.07±0.28	6.97%	2.98	3.83%
N076	2.46	0.172±0.014	2.76±0.23	12.20%	2.59	5.28%
N084	2.47	0.183±0.016	2.60±0.23	5.26%	2.59	4.86%
N092	2.63	0.175±0.016	2.72±0.25	3.42%	2.48	5.70%
N100	2.68	0.167±0.015	2.85±0.26	6.34%	2.68	0.00%

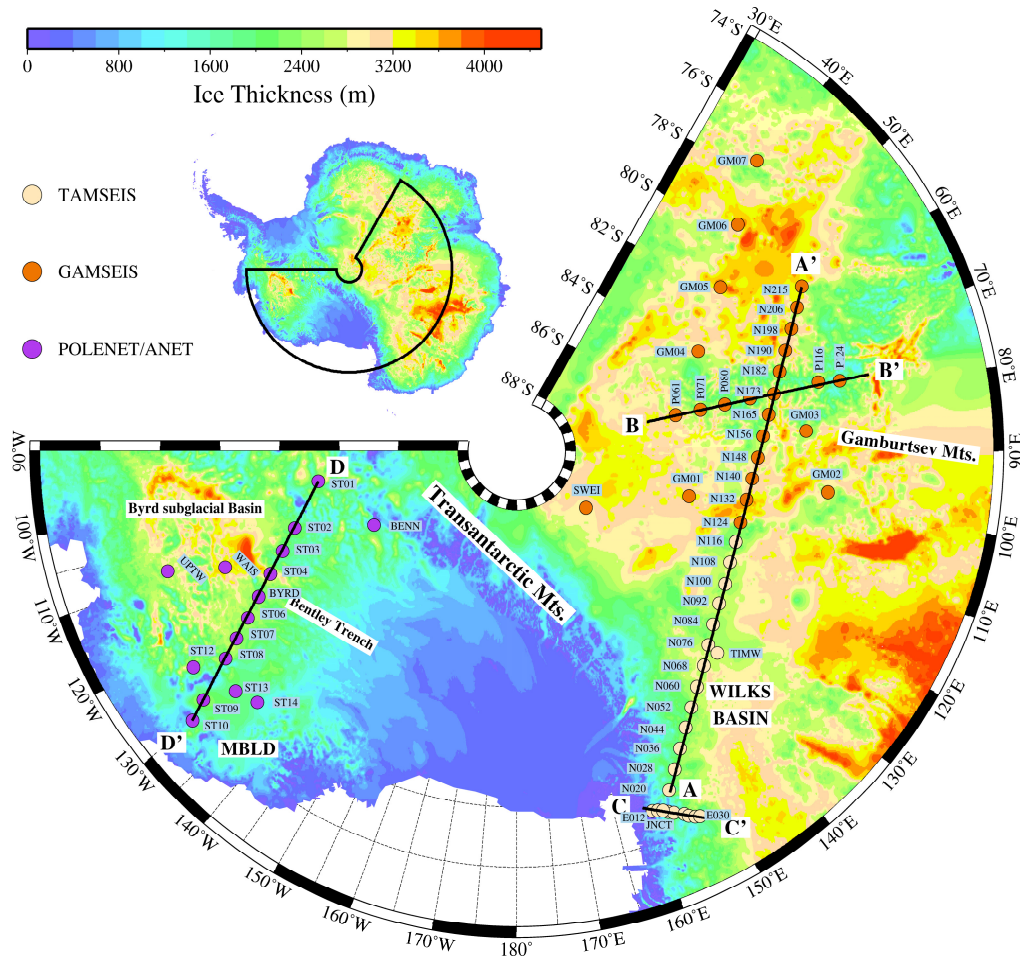
---

N108	2.45	0.177±0.014	2.68±0.21	9.39%	2.56	4.49%
N116	2.50	0.175±0.024	2.72±0.39	8.80%	2.46	1.60%

---

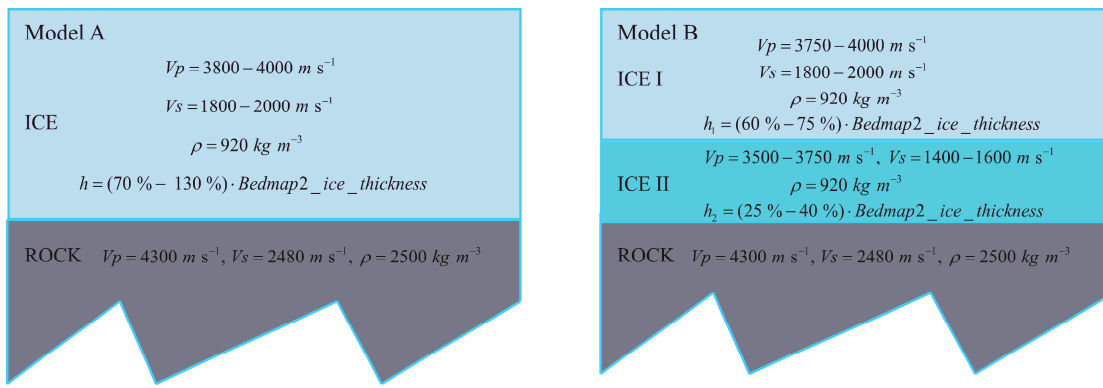
Table 1 (continued)

Station	Bedmap2 (km)	Resonance freq. (Hz)	<del>Thickness</del> <u>Equation (1)</u> (km)	Relative error	<del>Thickness</del> <u>HDFA+Model B</u> (km)	Relative error
N124	2.42	0.185±0.019	2.56±0.26	5.79%	2.57	6.20%
N132	3.24	0.146±0.018	3.26±0.40	0.62%	3.07	5.25%
N140	2.79	0.162±0.022	2.93±0.42	5.02%	2.69	3.58%
N148	2.9	0.137±0.017	3.46±0.44	19.31%	3.20	10.34%
N156	2.55	0.194±0.016	2.45±0.20	3.92%	2.48	2.75%
N165	2.81	0.150±0.021	3.16±0.44	12.46%	2.95	4.98%
N173	2.38	0.185±0.017	2.56±0.24	7.56%	2.54	6.72%
N182	2.42	0.191±0.014	2.49±0.19	2.89%	2.54	4.96%
N190	3.01	0.144±0.017	3.31±0.41	9.97%	3.15	4.65%
N198	3.32	0.148±0.017	3.21±0.38	3.31%	3.30	0.60%
N206	2.96	0.159±0.022	2.98±0.41	0.68%	2.61	11.82%
N215	3.48	0.155±0.017	3.07±0.33	11.78%	3.12	10.34%
P061	3.16	0.135±0.018	3.52±0.46	11.39%	3.17	0.63%
P071	2.3	0.194±0.018	2.45±0.23	6.52%	2.18	5.22%
P080	2.47	0.188±0.018	2.52±0.25	2.02%	2.52	2.02%
P090	2.34	0.212±0.022	2.24±0.23	4.27%	2.09	10.68%
P116	2	0.222±0.023	2.14±0.22	7.00%	1.93	3.50%
P124	1.54	0.314±0.033	1.51±0.16	1.95%	1.47	4.55%
ST01	3.02	0.157±0.015	3.02±0.28	0.00%	2.95	2.32%
ST02	2.12	0.164±0.018	2.89±0.32	36.32%	2.43	14.62%
ST03	<del>1.932.49</del>	0.236±0.019	2.01±0.16	<del>19.284.35%</del>	<del>2.861.96</del>	<del>14.861.33</del>
ST08	2.18	0.152±0.016	3.12±0.34	43.12%	2.50	14.68%
ST09	2.32	0.157±0.020	3.02±0.4	30.17%	2.66	14.66%
ST10	1.23	0.266±0.030	1.79±0.21	45.53%	1.51	22.76%
ST12	1.89	0.185±0.020	2.56±0.28	35.45%	2.15	13.76%
ST13	1.94	0.167±0.018	2.85±0.32	46.91%	2.23	14.95%
ST14	1.54	0.339±0.038	1.40±0.16	9.09%	1.44	6.49%
SWEI	2.84	0.162±0.017	2.93±0.31	3.17%	2.93	3.17%
TIMW	2.57	0.175±0.020	2.72±0.32	5.84%	2.65	3.11%
WAIS	3.37	0.127±0.015	3.73±0.43	10.68%	3.71	10.09%



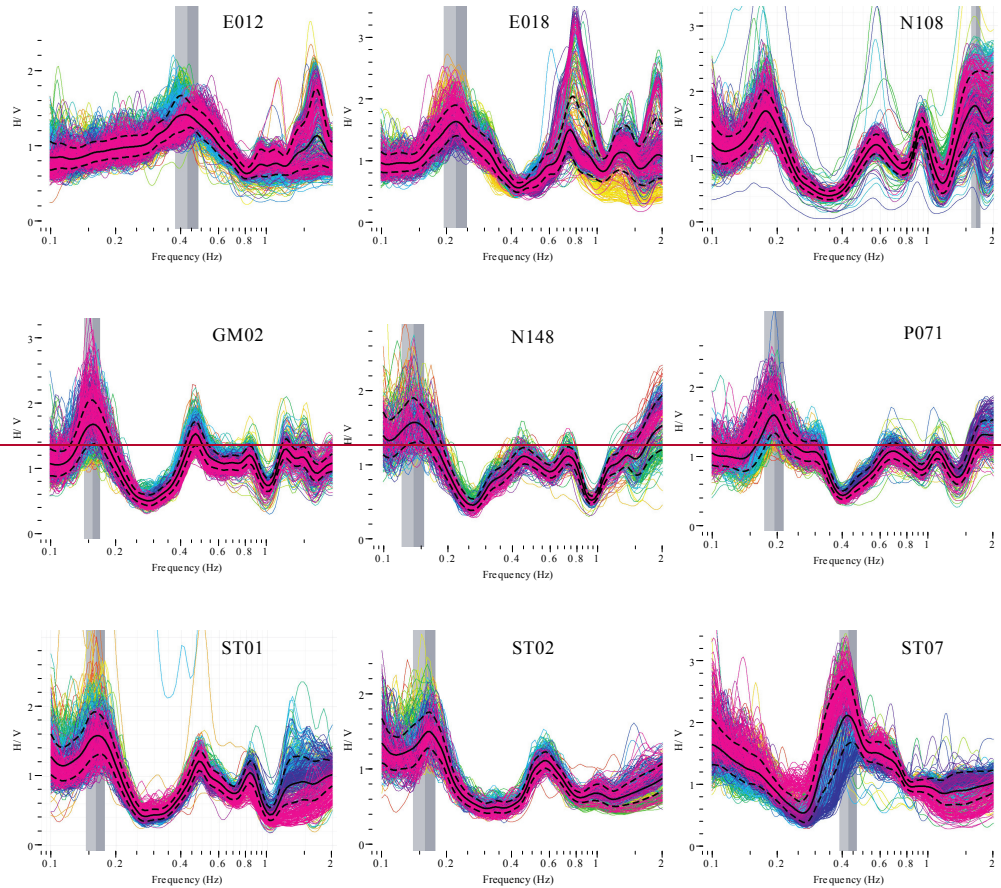
583  
584  
585  
586  
587  
588

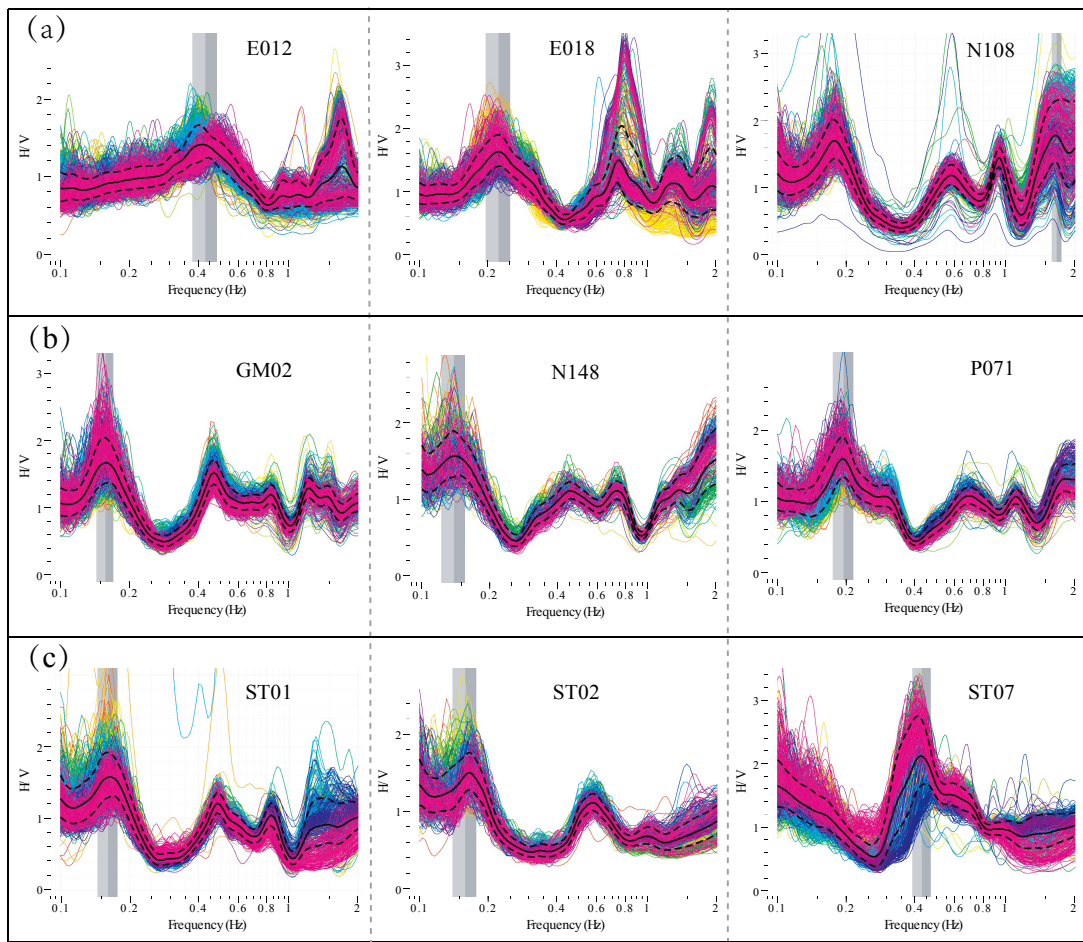
**Figure 1.** Locations of the three seismic arrays used in this study. Some stations are lined to four profiles marked with AA', BB', CC' and DD'. TAMSEIS: TransAntarctic Mountains Seismic Experiment; GAMSEIS: Gamburtsev Antarctic Mountains Seismic Experiment; POLENET/ANET: The Polar Earth Observing Network/Antarctic Network. Ice sheet thickness data in this plot come from Bedmap2 database.



**Figure 2.** Sketches of the two ice layer models used for H/V spectrum inversion. Model A comprises a single ice layer, while model B is a two-layer ice structure with low shear-wave velocity in the lower ice layer. The parameters used in the two models are consistent with ~~referred to~~ Wittlinger and Farra (2012).

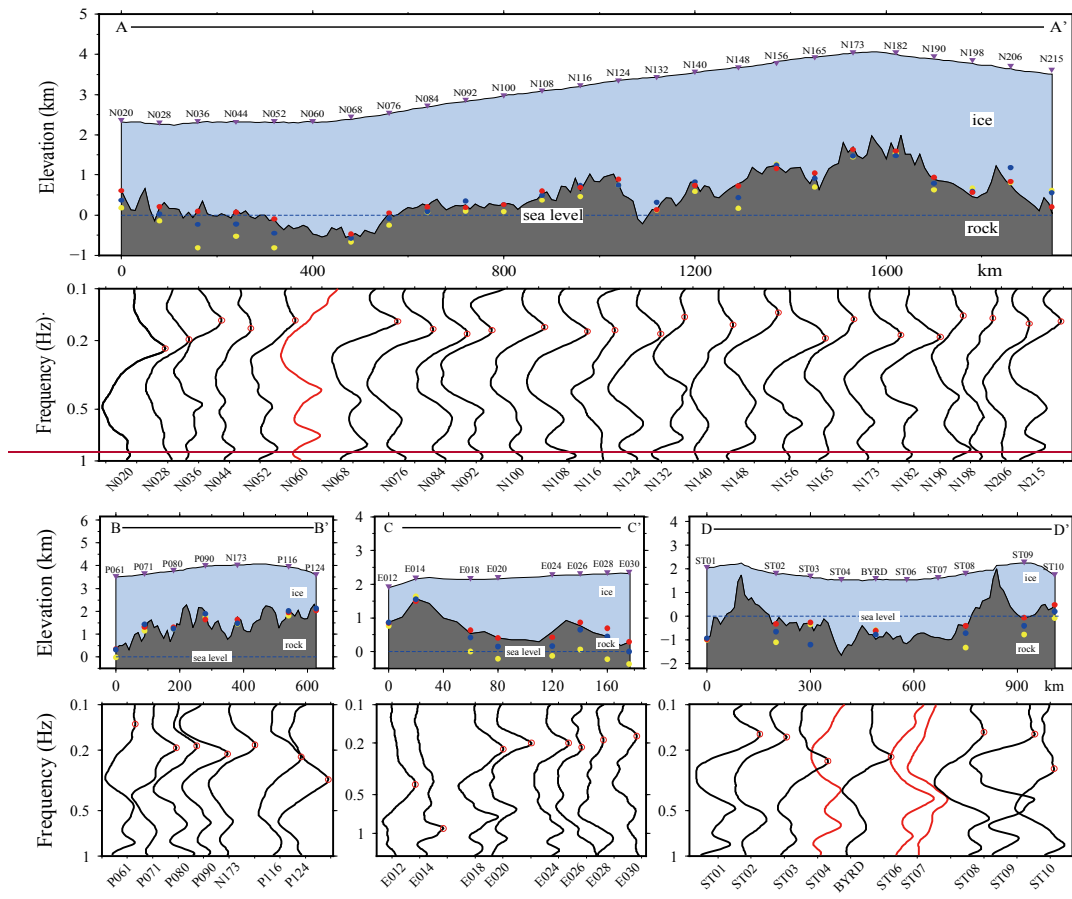




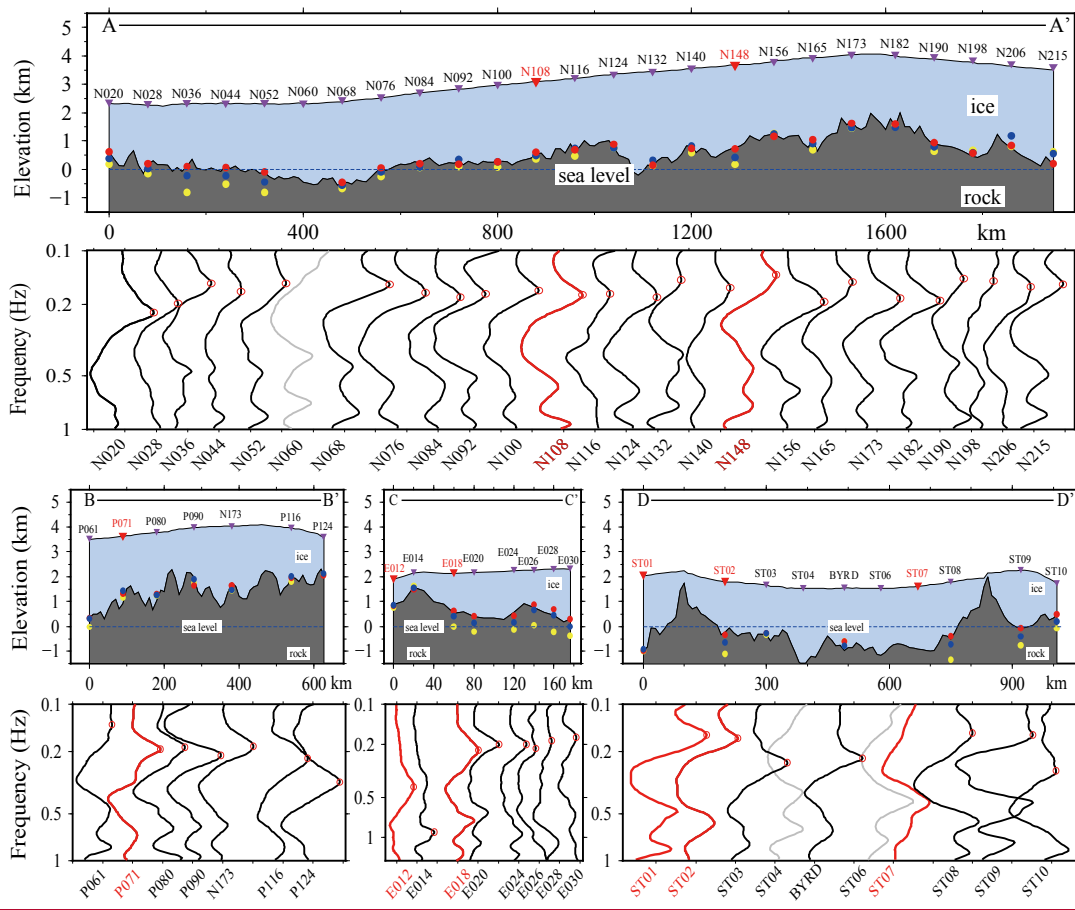


597  
 598 **Figure 3.** H/V spectra of nine stations shown as representative of all results in this study. Panel a, b, and c each is  
 599 comprised of three stations that belong to TAMSEIS, GAMSEIS, and POLENET/ANET array, respectively (The locations  
 600 can be seen in profiles displayed in Fig. 4). The H/V spectra were calculated using five-day long ambient noise record. In  
 601 each spectrum, the value at the limit between the two vertical gray areas is the peak frequency, while the two gray areas  
 602 denote its standard deviation. The spectra of the E012, E018, GM01, N148, P071, ST01 and ST02 stations represent 42  
 603 stations whose clear first peaks with the largest amplitudes are in agreement with the resonance frequency of the ice sheet  
 604 layer. Station N108 is representative of 18 stations whose first peaks are related to the ice sheet resonance frequency but  
 605 with slightly lower amplitude than peaks in higher frequencies. ST07 is the example that no peak frequency correlating to  
 606 the ice thickness appears as expected in the observed H/V spectrum.

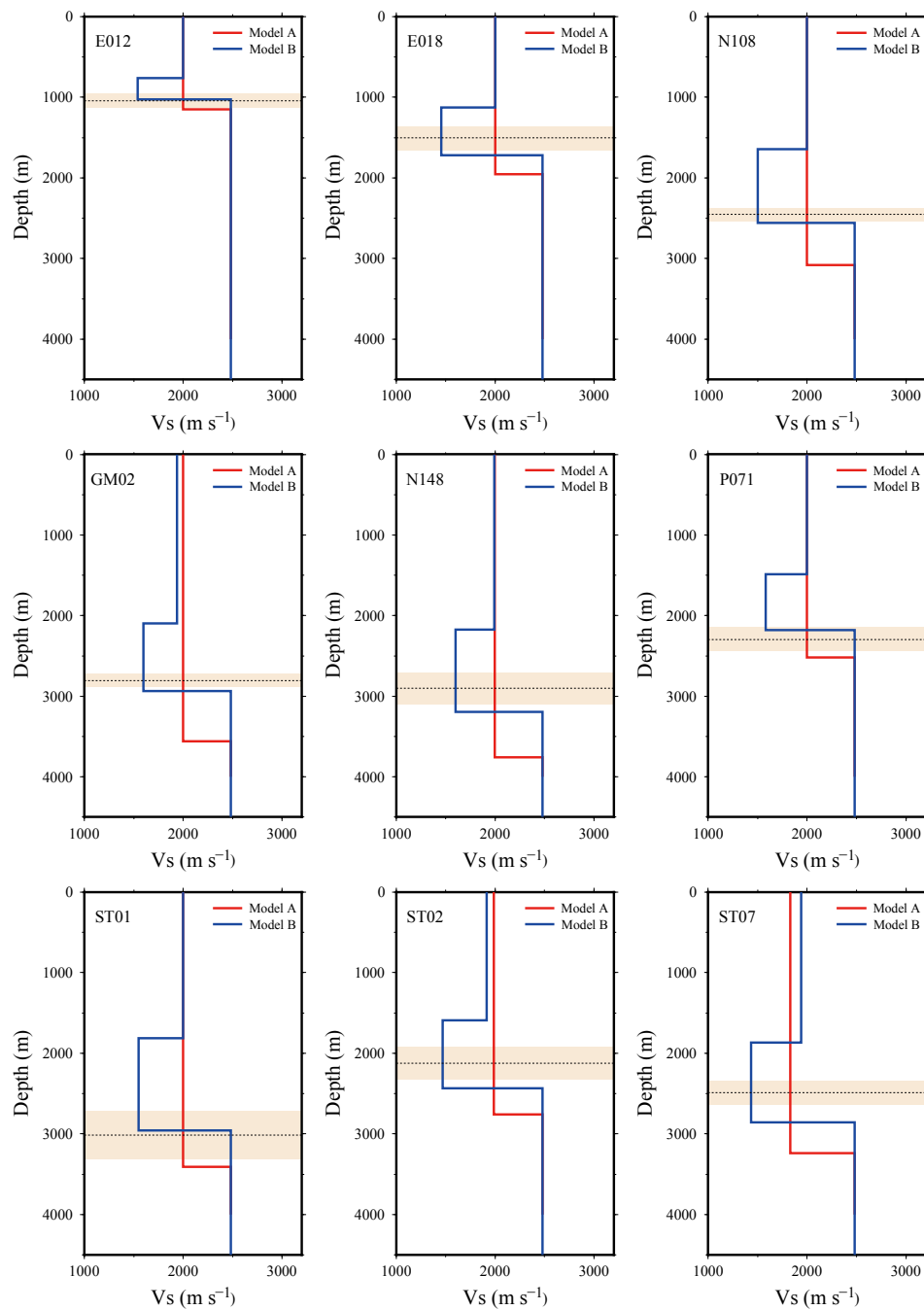




607



608  
 609 **Figure 4.** Cross section showing H/V spectra and the ice sheet thickness obtained from the H/V method at stations along  
 610 the four profiles (Fig. 1). In the below H/V spectra cross section panels, the red circles denote the resonance frequencies  
 611 correlating to the ice thickness for each station, and the spectra of the four stations without clear peaks are plotted with  
 612 gray lines. The spectra together with their station names that shown with red color, are correspondence to the stations  
 613 displayed in Fig. 3. The upper panels show the variation of the bedrock and ice surface elevation along each profile  
 614 obtained from Bedmap2 database. In these plots, the red dots indicate the reference Bedmap2 ice thickness, while the  
 615 yellow and the blue dots represent the Equation (1) estimates calculated ice thickness using Eq. (1) and the DFA + Model  
 616 B estimates the inversion ice thickness from model B, respectively.  
 617



619

620

621

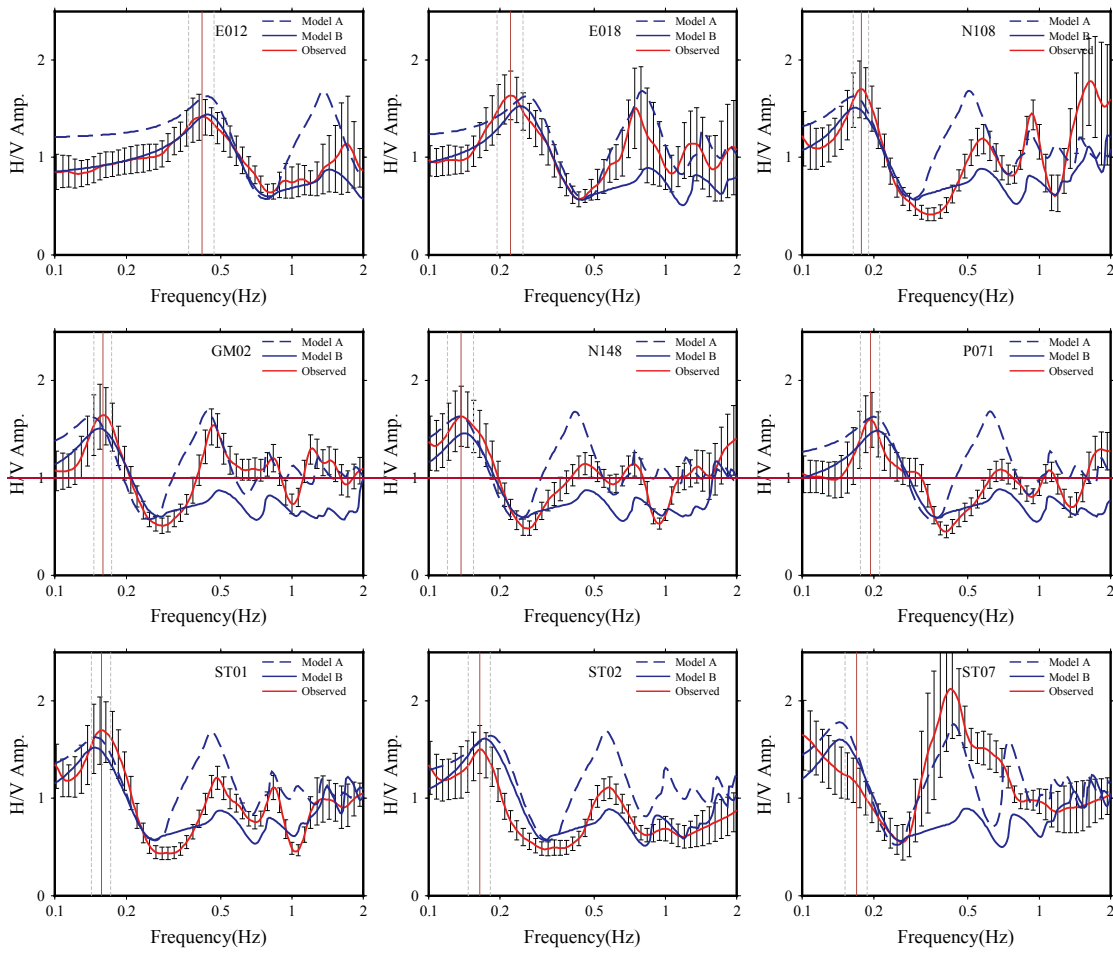
622

623

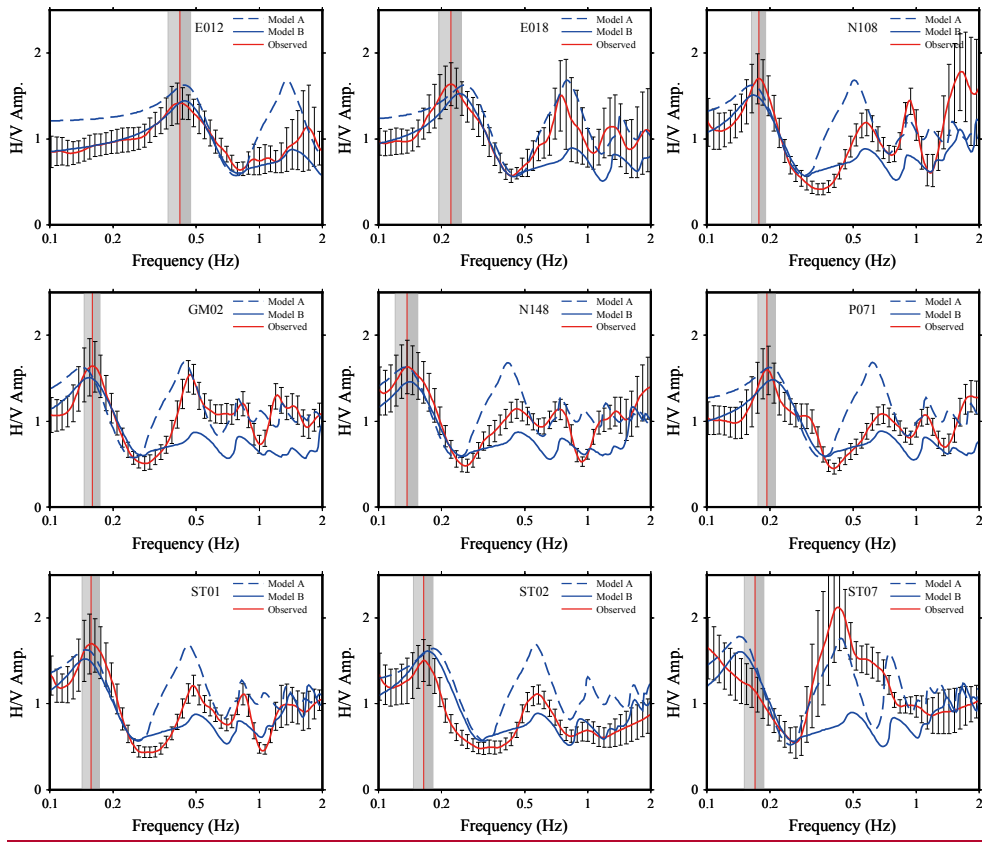
624

**Figure 5.** The optimum inversion shear-wave velocity models for the nine stations. The horizontal dashed line in each plot indicates the reference Bedmap2 ice thickness, and the shaded area shows the uncertainty of the Bedmap2 ice thickness. Apparently, the inversion ice thickness results derived from the two-layer structure (model B) are much closer to the Bedmap2 thickness than those determined using the single ice layer (model A).





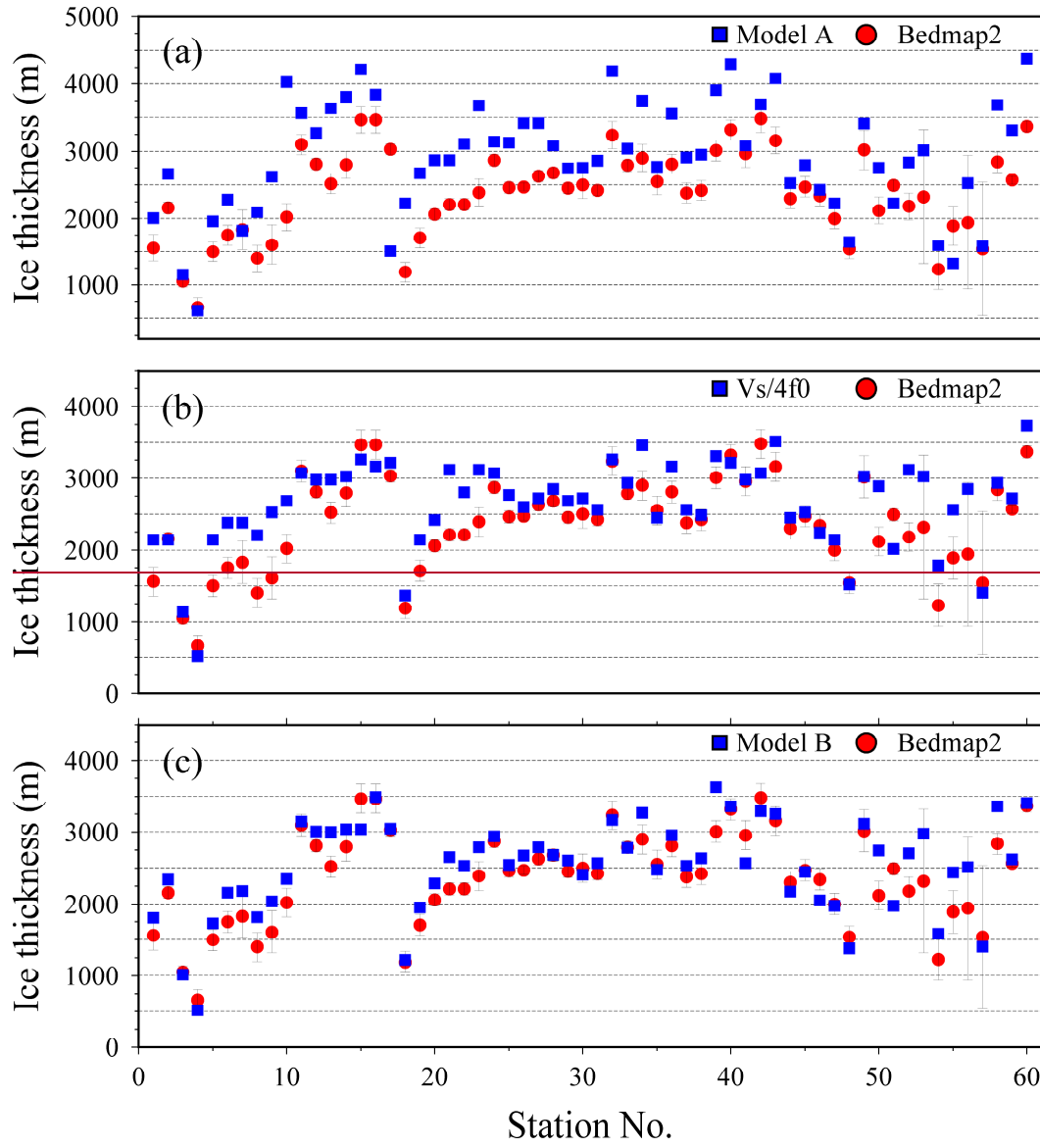
626



627  
628  
629  
630  
631  
632  
633  
634  
635

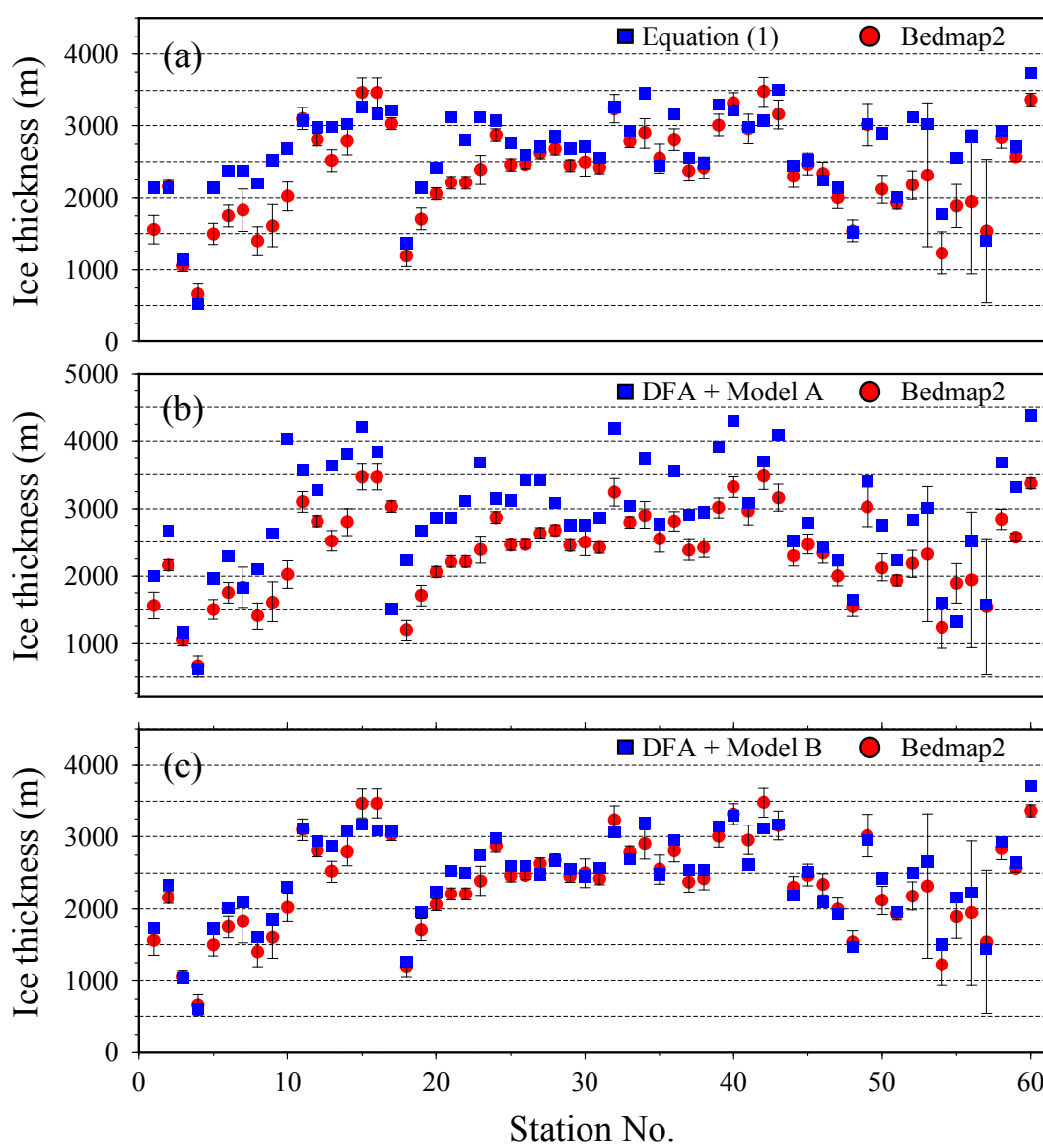
**Figure 6.** The synthetic H/V spectra and the observed H/V spectrum for the nine stations. The synthetic H/V spectra are modelled using the optimum inversion shear-wave velocity profiles for model A and model B. In all plots except for the last one, the vertical bars are the same as those in Fig.3 (i.e. the real peak frequency and the associated standard deviation). As for the last one, the peak frequency is approximately calculated using Eq. (1) with its Bedmap2 ice thickness, and the deviation is also approximated with a relative error of 10 % to its peak frequency. The two synthetic H/V spectra are both in good agreement with the observed H/V spectrum. Note that the amplitudes of the synthetic H/V spectra are normalized by dividing 2 in the whole frequency band.





637

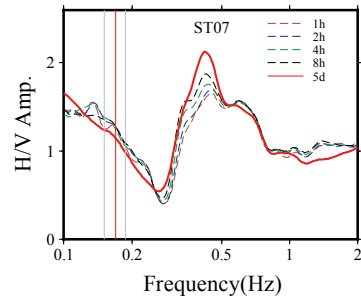
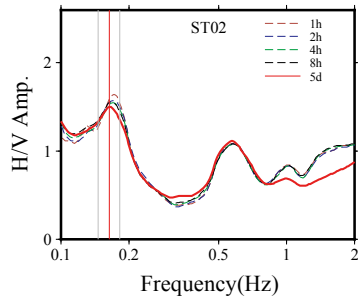
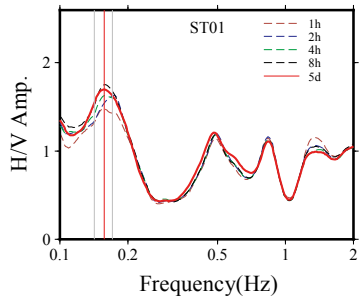
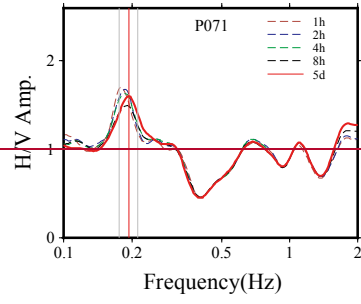
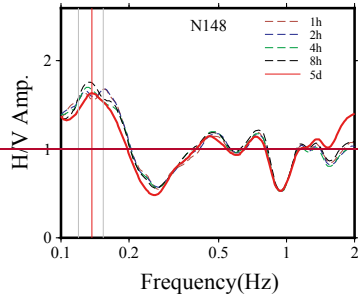
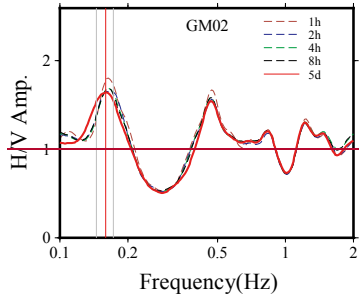
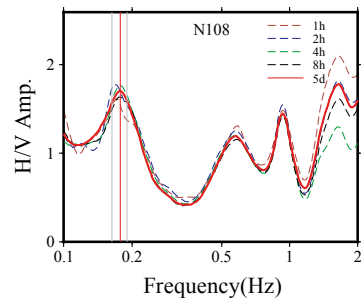
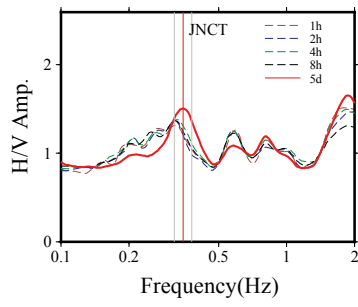
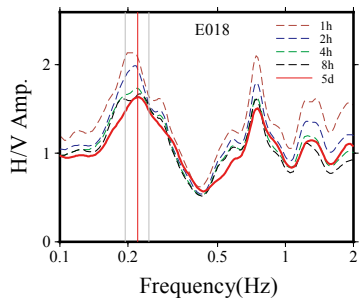




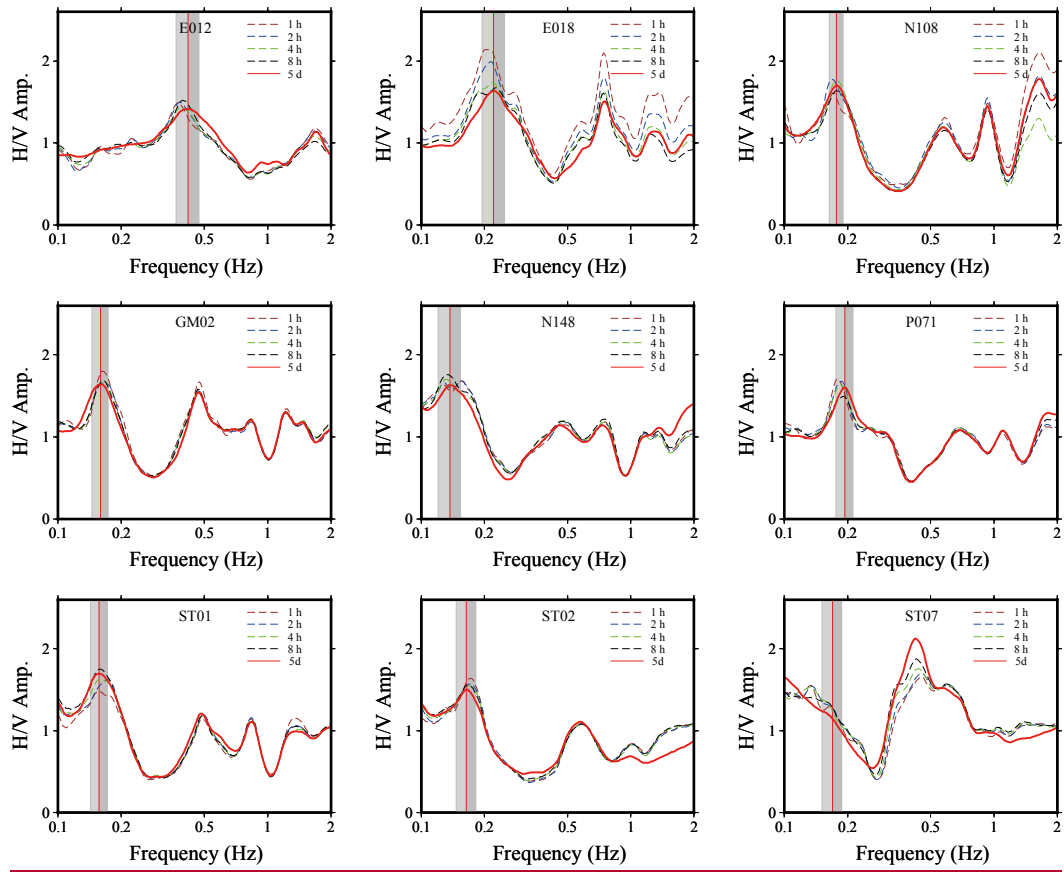
638  
639  
640  
641  
642  
643  
644

**Figure 7.** Ice thickness derived from the H/V method versus the reference Bedmap2 ice thickness. The station number of this figure is in the same order of the stations listed in Table 1. The blue squares in panel (a), (b), and (c) represent Equation (1)-ice thickness estimations from model A, Eq. (1), and model B, DFA + Model A, and DFA + Model B estimates, respectively. The red circles in each panel denote the Bedmap2 ice thickness and each Bedmap2 value is marked with its corresponding error bar obtained from the uncertainty grids (Fretwell et al., 2013).





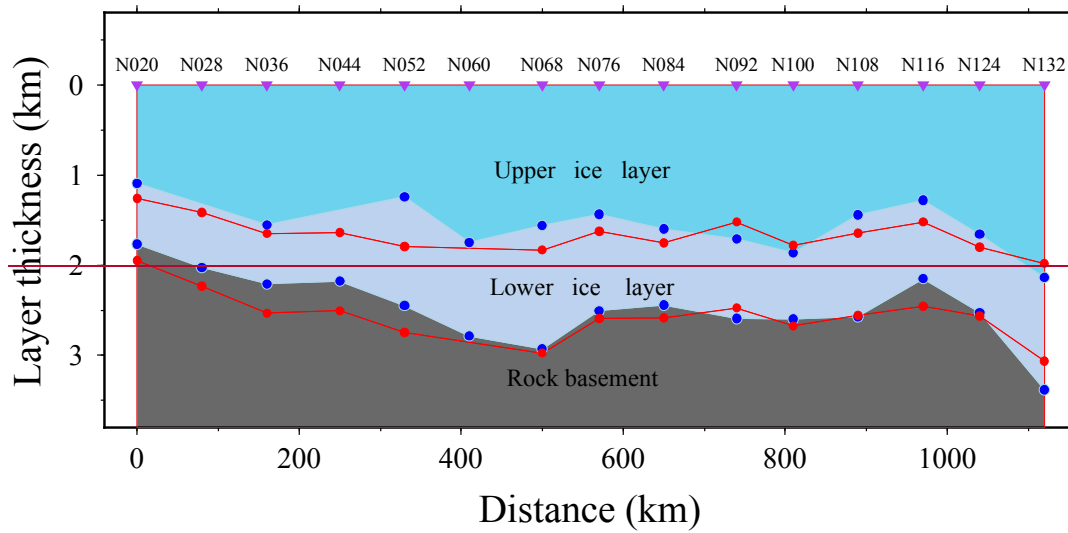
646



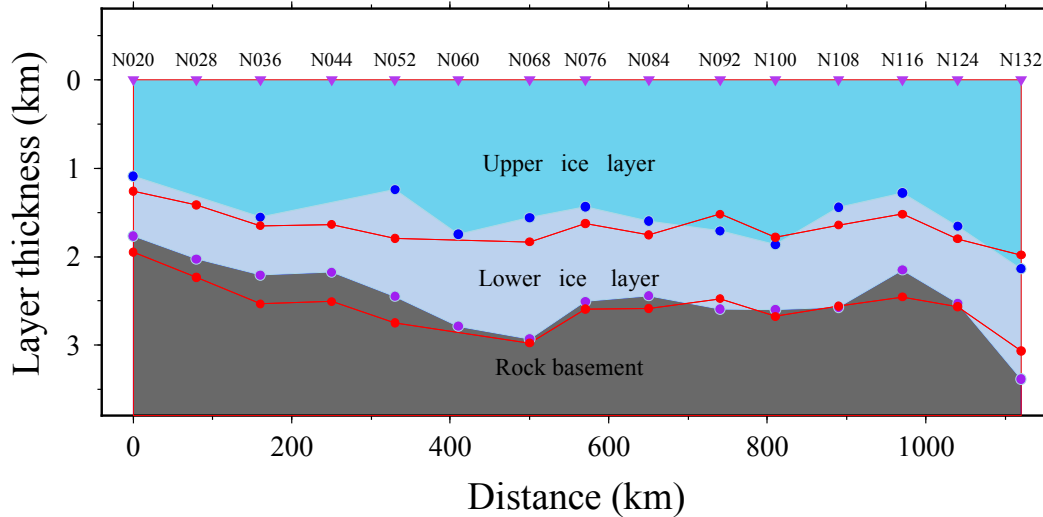
647  
648  
649  
650  
651  
652  
653  
654

**Figure 8.** H/V spectra calculated using different lengths of ambient noise records. The vertical bars in all panels except for the last one represent the peak frequencies and the corresponding standard deviations the same as those in Fig. 3 and Fig. 6. There is a good consistence between H/V spectra determined with different tesing length of noise records (1 h, 2 h, 4 h and 8 h) and the spectrum with record five-day long, both in locations of peak frequencies and the spectra shape. However, the peak frequency obtained from 1 h record slightly deviates the peak frequency determined using 5 d record for the E012 station.

655



656



657

658

659

660

661

662

663

664

665

**Figure 9.** Comparisons of the two-layer ice sheet structure thickness results obtained from our study and Wittlinger and Farra (2012)'s. The red dots shown in shallower depth denote the interface between the upper and the lower ice sheet obtained in this study. The interface is generally consistent with that ice thickness derived from H/V spectrum inversion in our study (as the blue dots shown), and the blue dots indicate the ice thickness determined with the PRF method and a grid search stacking technique (Wittlinger and Farra, 2012, Table\_1). The red dots shown in deeper depth represent the overall ice thickness derived from model B, which is also consistent with the radar ice thickness (as the purple dots shown) adopted by Wittlinger and Farra (2012).